

AD-A037 471

AIR FORCE FLIGHT DYNAMICS LAB WRIGHT-PATTERSON AFB OHIO F/G 20/4  
APPLICATION OF THE INITIAL PLUME ANGLE CORRELATION TO CORRECT N--ETC(U)  
DEC 76 D L BOWERS

UNCLASSIFIED AFFDL-TR-76-138

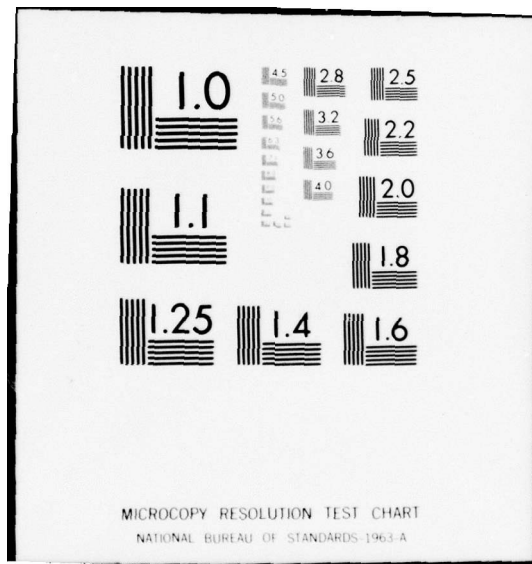
NL

1 of 1  
ADA037471



END

DATE  
FILMED  
4-77



ADA037471

AFFDL-TR-76-138

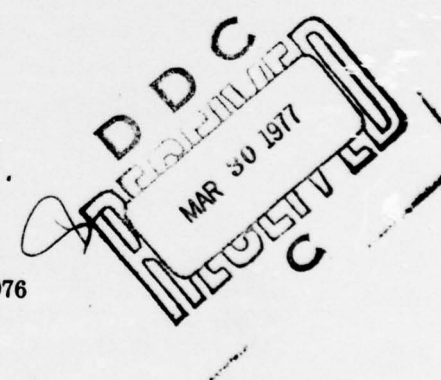
*[Handwritten signature]* *12*

## APPLICATION OF THE INITIAL PLUME ANGLE CORRELATION TO CORRECT NOZZLE/AFTBODY PRESSURE DRAG FOR HOT EXHAUST GAS EFFECTS

AERODYNAMICS AND AIRFRAME BRANCH  
AEROMECHANICS DIVISION

DECEMBER 1976

TECHNICAL REPORT AFFDL-TR-76-138  
FINAL REPORT FOR PERIOD JANUARY 1976 - SEPTEMBER 1976



Approved for public release; distribution unlimited

*WW WW.*  
DDC FILE COPY

AIR FORCE FLIGHT DYNAMICS LABORATORY  
AIR FORCE WRIGHT AERONAUTICAL LABORATORIES  
AIR FORCE SYSTEMS COMMAND  
WRIGHT-PATTERSON AIR FORCE BASE, OHIO 45433

NOTICE

When Government drawings, specifications, or other data are used for any purposes other than in connection with a definitely related Government procurement operation, the United States Government thereby incurs no responsibility nor any obligation whatsoever; and the fact that the government may have formulated, furnished, or in any way supplied the said drawings, specifications, or other data, is not to be regarded by implication or otherwise as in any manner licensing the holder or any other person or corporation, or conveying any rights or permission to manufacture, use, or sell any patented invention that may in any way be related thereto.

This report has been reviewed by the Information Office (OI) and is releasable to the National Technical Information Services (NTIS). At NTIS, it will be available to the General Public, including foreign nations.

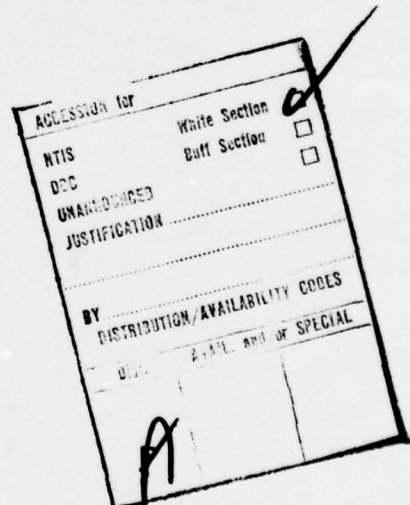
This technical report has been reviewed and is approved for publication.

*Douglas L. Bowers*  
DOUGLAS L. BOWERS  
Project Engineer

FOR THE COMMANDER

*Alfred C. Draper*  
ALFRED C. DRAPER  
Assistant for Research and Technology  
Aeromechanics Division

AIR FORCE - 23 MARCH 77 - 100



UNCLASSIFIED

SECURITY CLASSIFICATION OF THIS PAGE (When Data Entered)

DD FORM 1 JAN 73 1473 EDITION OF 1 NOV 65 IS OBSOLETE

**UNCLASSIFIED**

SECURITY CLASSIFICATION OF THIS PAGE (When Data Entered)

012 070

UNCLASSIFIED

SECURITY CLASSIFICATION OF THIS PAGE(When Data Entered)

results from other sources of hot exhaust jet data relating to ratio of specific heat effects, temperature effect on exhaust plume spreading, and the effect of body heating on external nozzle boattail performance.



UNCLASSIFIED

SECURITY CLASSIFICATION OF THIS PAGE(When Data Entered)

FOREWORD

This report was prepared by Douglas L. Bowers of the Internal Aerodynamics Group, Aerodynamics and Airframe Branch, Aeromechanics Division of the Air Force Flight Dynamics Laboratory, Wright-Patterson Air Force Base, Ohio. This research was conducted under Work Unit Number 14760221, "Design and Analysis of Advanced Strategic and Tactical Military Aircraft Exhaust Nozzle Systems". This research was conducted from 1 January 1976 to 1 September 1976.

(This page intentionally left blank.)

## TABLE OF CONTENTS

SECTION		PAGE
I	INTRODUCTION	1
II	DISCUSSION	3
	1. Basic Aftbody Nozzle Flow Parameters	3
	2. Effect of Temperature Variation on Exhaust Plume $\delta_j$	8
	3. Effect of Exhaust Plume $\delta_j$ on Aftbody Nozzle Performance	10
	4. Correction of Cold Exhaust Gas Data for Hot Exhaust Gas Effects	10
	5. Calculation of $\delta_j$ and Construction of the $\delta_j$ vs NPR Plot	16
	6. Survey of Available Experimental Data Applicable to Hot Exhaust Gas Effects	26
III	SUMMARY	67
	BIBLIOGRAPHY	69
	REFERENCES	70

## LIST OF FIGURES

FIGURE	PAGE
1 Basic Geometric Parameters for Nozzle Flow	4
2 Nozzle Flow-Subsonic Freestream Mach Number	5
3 Nozzle Flow-Supersonic Freestream Mach Number	7
4 (Reference 4) Initial Plume Angle vs. Static Pressure Ratio	9
5 (Reference 5) Effect of the Ratio of Specific Heats upon the Variation in Prandtl-Meyer Turning Angle	11
6 (Reference 5) Effect of the Ratio of Specific Heats upon the Variation in the Ratio of Static to Stagnation Pressure with Mach Number	12
7 (Reference 7) Effect of Nozzle Plume Simulators on Aftbody Drag	13
8 (Reference 1) Drag Coefficient Sensitivity with Temperature	14
9 (Reference 2) Aftbody Drag Sensitivity	15
10 Drag Coefficient and Initial Plume Angle vs NPR	17
11 Nozzle Exit Flow - $\delta_j$ Definition	23
12 Internal Nozzle Exit Flow - $\delta_j = 0$	23
13 External Nozzle Exit Flow - $\delta_j = 0$	23
14 Sample Supersonic Freestream Calculation	24
15 Pressure/Deflection Match Point	25
16 (Reference 1) Basic Model Dimensions and Location in Test Section	27
17 (Reference 1) Model Details	28
18 Aftbody Pressure Drag Sensitivity with Temperature, $M_\infty = 0.9$	29
19 (Reference 1) Effect of Exhaust Plume Temperature at $M_\infty = 0.9$	30

## LIST OF FIGURES (CONT'D)

FIGURE	PAGE
20 Initial Plume Angle Correlation, Reference 1 Data, $M_{\infty}=0.9$	32
21 Drag Coefficient vs. NPR, Reference 1 Data, $M_{\infty}=1.5$	33
22 Initial Plume Angle Correlation, Reference 1 Data, $M_{\infty}=1.5$	34
23 Drag Coefficient vs. NPR and Initial Plume Angle Correlation, Reference 9 Data, 15° Boattail, $M_{\infty}=0.8$	35
24 Drag Coefficient vs. NPR and Initial Plume Angle Correlation, Reference 9 Data, 15° Boattail, $M_{\infty}=0.9$	37
25 Drag Coefficient vs. NPR and Initial Plume Angle Correlation, Reference 9 Data, 15° Boattail, $M_{\infty}=1.1$	39
26 Drag Coefficient vs. NPR and Initial Plume Angle Correlation, Reference 9 Data, 25° Boattail, $M_{\infty}=0.8$	42
27 Drag Coefficient vs. NPR and Initial Plume Angle Correlation, Reference 9 Data, 25° Boattail, $M_{\infty}=0.9$	44
28 (Reference 2) Nozzle Details	46
29 (Reference 2) Pressure Distribution for Hot Exhaust Jets	48
30 (Reference 2) Drag Coefficient Sensitivity, $M_{\infty}=0.9$	49
31 (Reference 2) Drag Coefficient Sensitivity, $M_{\infty}=1.20$	50
32 (Reference 8) Test Apparatus and Nozzle Models	51
33 (Reference 8) Drag Coefficient vs. NPR and Initial Plume Angle Correlation, $M_{\infty}=0.8$	52
34 (Reference 8) Drag Coefficient vs. NPR and Initial Plume Angle Correlation, $M_{\infty}=0.9$	54
35 (Reference 12) Basic Model Details	58
36 (Reference 11) Effect of $\gamma$ and Temperature Variations on Base Pressure Coefficient	59

LIST OF FIGURES (CONCLUDED)

FIGURE	PAGE
37 (Reference 13) Model Details and Rake Position	61
38 (Reference 13) Mach Number Profiles for Cold and Hot Exhaust Jets	62
39 (Reference 14) Drag Coefficient Sensitivity with Temperature	64
40 (Reference 14) External Nozzle Aftbody Pressure Coefficient Distribution Variations with Exhaust Plume Temperature	65
41 (Reference 15) Drag Coefficient Sensitivity with Exhaust Jet Temperature	66

## LIST OF SYMBOLS

A - cross-sectional area

$C_D$  - aftbody drag coefficient based on maximum body cross-sectional area (unless otherwise noted)

$C_p$  - pressure coefficient,  $\frac{P - P_\infty}{q}$

F - degrees Fahrenheit

R - degrees Rankine

NPR - nozzle pressure ratio:  $P_T/P_\infty$

M - Mach number

m - meter

P - static pressure

$P_T$  - total pressure at nozzle throat

$\theta$  - local flow direction

$\delta$  - flow turning angle

$\nu$  - Prandtl-Meyer function

$\mu$  - Mach angle:  $\mu = \sin^{-1} \frac{1}{M}$

$\gamma$  - Ratio of specific heats

LIST OF SYMBOLS (CONT'D)

subscripts

- e - nozzle exit
- Th - nozzle throat
- j - exhaust plume
- $\infty$  - freestream
- BT - boattail or base
- N - internal nozzle
- I - internal nozzle
- E - freestream

superscripts

- \* - station corresponding to sonic flow

SECTION I  
INTRODUCTION

The requirement for advanced aircraft airframe systems and advanced propulsion systems has resulted in extensive efforts in analytical and experimental system development. In the exhaust nozzle area, this effort has produced configurations as simple as the nozzles of the 1945 vintage P-80 "Shooting Star" and the 1949 vintage F-84 "Thunderjet" and as complex as the blow-in-door ejector nozzles of the 1964 vintage F-111 and F-12 and balanced beam nozzle of 1972 vintage F-15 and F-16. As exhaust nozzle systems become more complicated, the required wind tunnel models necessarily become more complex and costly. Limited by resources and manufacturing capability, wind tunnel model propulsion systems are simulated by high pressure cold air systems. This simulation has produced adequate results by neglecting the effect of a hot exhaust gas composed of jet fuel combustion products on external aftbody nozzle performance. Previous experimental work (References 1, 2) has indicated that changes in exhaust gas temperature (or ratio of specific heats) alter the exhaust plume shape, especially the initial plume inclination angle. Attempts to correct cold jet aftbody performance for hot exhaust jet effects using the initial plume angle as a correlating parameter have been reasonably successful for a limited data base. This document describes the application of the initial plume angle correlation for hot jet exhaust effects to an extended data base, i.e., all available applicable hot exhaust jet data produced from 1953 to the present time. Also presented are pertinent results from other hot exhaust gas nozzle test programs which give insight to the overall effect of temperature or ratio of specific heat variations on nozzle boattail performance. Described is the general aftbody

AFFDL-TR-76-138

flow problem, the methods of calculating the initial plume inclination angle, the experimental data, and application of the correlation. Data analysis was conducted from 1 January 76 to 1 September 76.

## SECTION II

## DISCUSSION

## 1. BASIC AFTBODY NOZZLE FLOW PARAMETERS

The basic geometric parameters for nozzle flow are described in Figure 1. The nozzle contour shown is for a convergent divergent nozzle.  $\theta_{BT}$  is the trailing edge nozzle external boattail angle,  $\theta_N$  is the nozzle internal divergence angle, and  $\delta_j$  is the initial plume inclination angle measured from the nozzle exit. The  $\delta_j$  value is defined for supersonic flow exhaust plumes only. The geometric areas are  $A_T$ , nozzle throat area and  $A_e$ , nozzle exit area. Flow parameters are  $P_T$ , nozzle throat total pressure,  $P_e$ , nozzle internal static pressure at nozzle exit,  $P_j$ , static pressure at nozzle exit after internal expansion,  $M_e$ , Mach number at nozzle exit,  $M_j$ , Mach number after internal expansion at nozzle exit,  $P_{BT}$ , boattail or base static pressure,  $P_\infty$ , freestream static pressure, and  $M_\infty$ , freestream Mach number. The ratio of specific heats,  $\gamma$ , is subscripted "I" for the internal flow and "E" for the freestream flow.

For jets exiting into a subsonic stream the internal flow can assume four conditions; 1) all subsonic, 2) mixed subsonic/supersonic flow, 3) all supersonic with perfect expansion and 4) all supersonic and underexpanded. For the all subsonic case, Figure 2a, (internal and external flow), the static pressure at the exit is matched internally and externally. In Figure 2b, the nozzle total pressure is sufficient to have choked flow at the nozzle throat and  $M>1$  flow in a section of the diverging section. The static pressure at the exit of the nozzle is matched internally and externally by a combination of the normal shock and the subsonic expansion in the remaining divergent section. In condition 2c, the pressure is matched with a normal shock at the exit. In these three cases 2a, 2b, and 2c, the nozzle exit flow is similar and an initial plume inclination angle

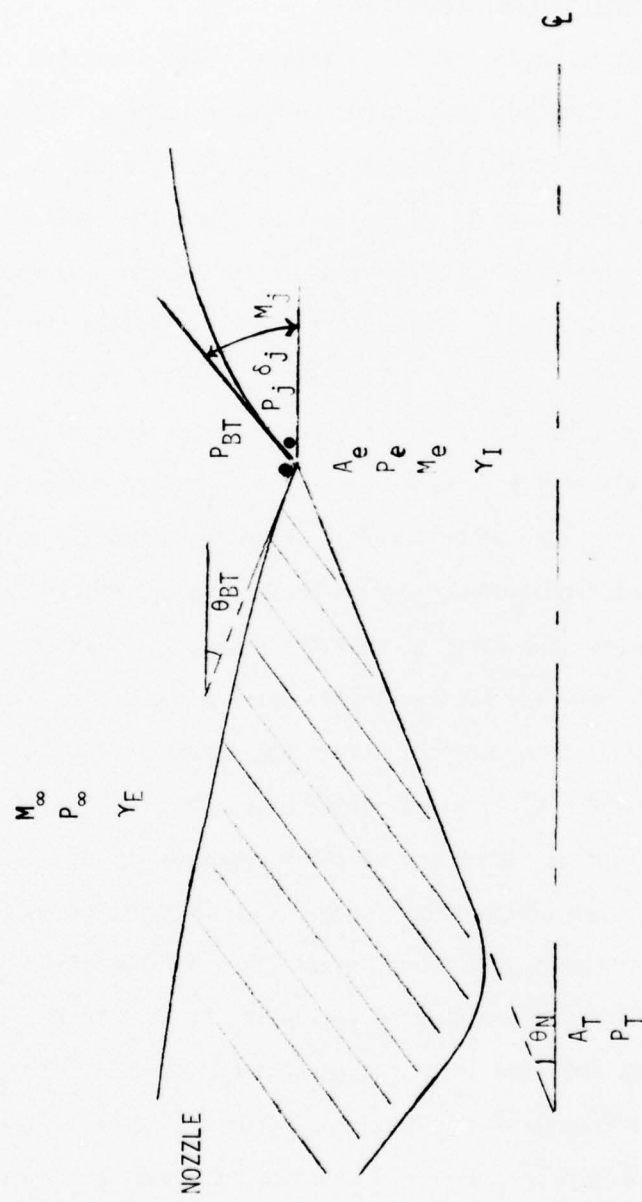


Figure 1. Basic Geometric Parameters for Nozzle Flow

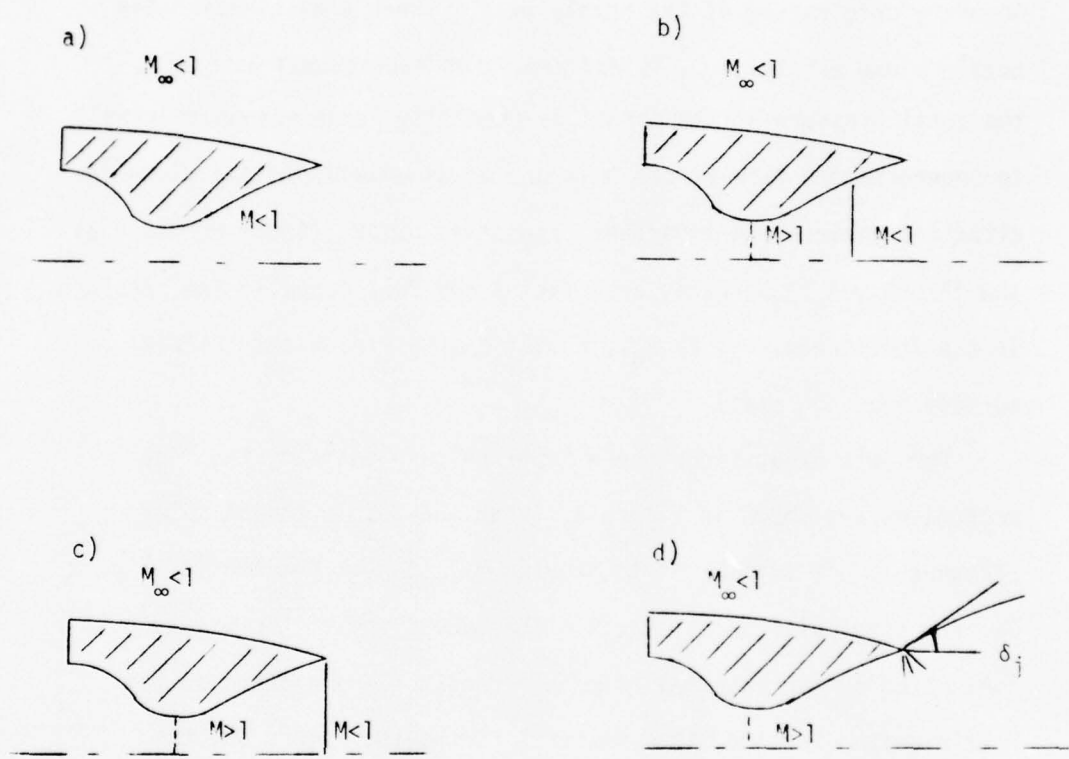


Figure 2. Nozzle Flow - Subsonic Freestream Mach Number

$\delta_j$  is not defined. The case where the  $\delta_j$  is defined is shown in Figure 2d. The static pressure in the nozzle at the exit after the internal expansion is still greater than the freestream static pressure. In this case, the flow expands to create the plume boundary originating at the nozzle exit. When a distinguishable nozzle plume exists, a  $\delta_j$  is defined. For operational aircraft, the total pressure at the throat is generally large enough to result in underexpanded flow at the exit and a subsequent initial plume inclination angle. The important parameters are  $P_T$  (total pressure at the throat),  $A_E/A_T$  (nozzle area ratio) and  $P_{REF}$  (usually the pressure in the freestream,  $P_\infty$ , or  $P_{BT}$ , a static pressure on the external surface near the exit).

For jets exhausting into a supersonic freestream, the flow mechanisms are shown in Figure 3. When the nozzle throat total pressure is not sufficient to provide  $M=1$  flow at the throat, Figure 3a, the internal flow is subsonic throughout and static pressure is controlled by the external reference pressure and matched at the nozzle exit. For the mixed internal flow case, Figure 3b, the internal normal shock location and the amount of subsonic expansion interact with the external supersonic flow after an oblique shock or expansion system to match static pressure and direction at the nozzle exit. To solve this case for the correct combination of normal shock location and external flow oblique shock or expansion system becomes a complicated problem dependent on throat total pressure, nozzle area ratio, and external reference pressure. In example 3c, the flow is supersonic throughout. The matching of static pressure and flow

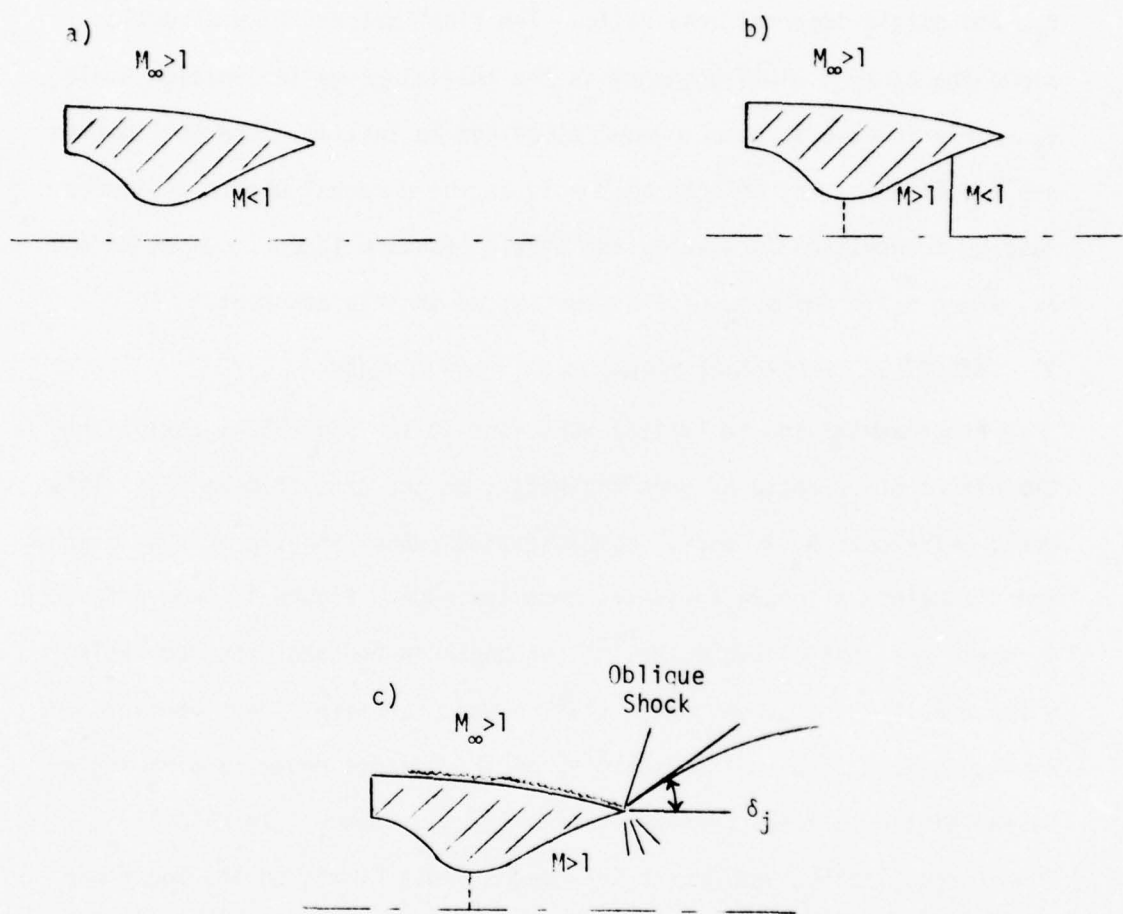


Figure 3. Nozzle Flow - Supersonic Freestream Mach Number

direction at the nozzle exit is accomplished by oblique shock or expansion wave systems and is dependent on the external reference pressure, external nozzle boattail angle,  $\theta_{BT}$ , internal nozzle divergence angle,  $\theta_N$ , and nozzle internal area ratio. The final matched flow direction along the exhaust plume boundary is the initial plume inclination angle,  $\delta_j$ . Only in case 3c is an exhaust plume and an initial plume inclination angle defined. Any effects of the  $\delta_j$  on the external nozzle pressures must be transmitted forward by the nozzle boundary layer. Cases 2d and 3c, where  $\delta_j$  is defined, will be emphasized in this document.

## 2. EFFECT OF TEMPERATURE VARIATION ON EXHAUST PLUME $\delta_j$

Experimental and analytical work done in the mid-1950's established the effect of  $\gamma$ , ratio of specific heats, on the exhaust plume  $\delta_j$ . This work, References 3, 4, and 5, combined wind tunnel Schlieren photographs and the method of characteristics computer code. Figure 4, from Reference 4, shows the initial plume inclination angle increasing with decreasing  $\gamma$  for a  $M_j=2.0$  and at any given static pressure ratio. This variation of  $\delta_j$  with  $\gamma$  is a result of sensitivity of the Prandtl-Meyer turning angle,  $\nu$ , and static to total pressure ratio,  $(P/P_T)$ , with  $\gamma$ . In NACA 1135, "Equations, Tables, and Charts For Compressible Flow", pg 14, Equations 171a and 173c are the following relations:

$$\nu = \left(\frac{\gamma+1}{\gamma-1}\right)^{1/2} \tan^{-1} \left(\frac{\gamma-1}{\gamma+1} (M^2 - 1)\right)^{1/2} - (90^\circ \mu)$$

$$\left(\frac{P}{P_T}\right)^{\frac{\gamma-1}{\gamma}} = \frac{1}{\gamma+1} \left(1 + \cos\left(2 \left[\frac{\gamma-1}{\gamma+1}\right]^{1/2} \left(\nu + \tan^{-1} \left(\frac{\gamma-1}{\gamma+1} (M^2 - 1)^{1/2}\right)\right)\right)\right)$$

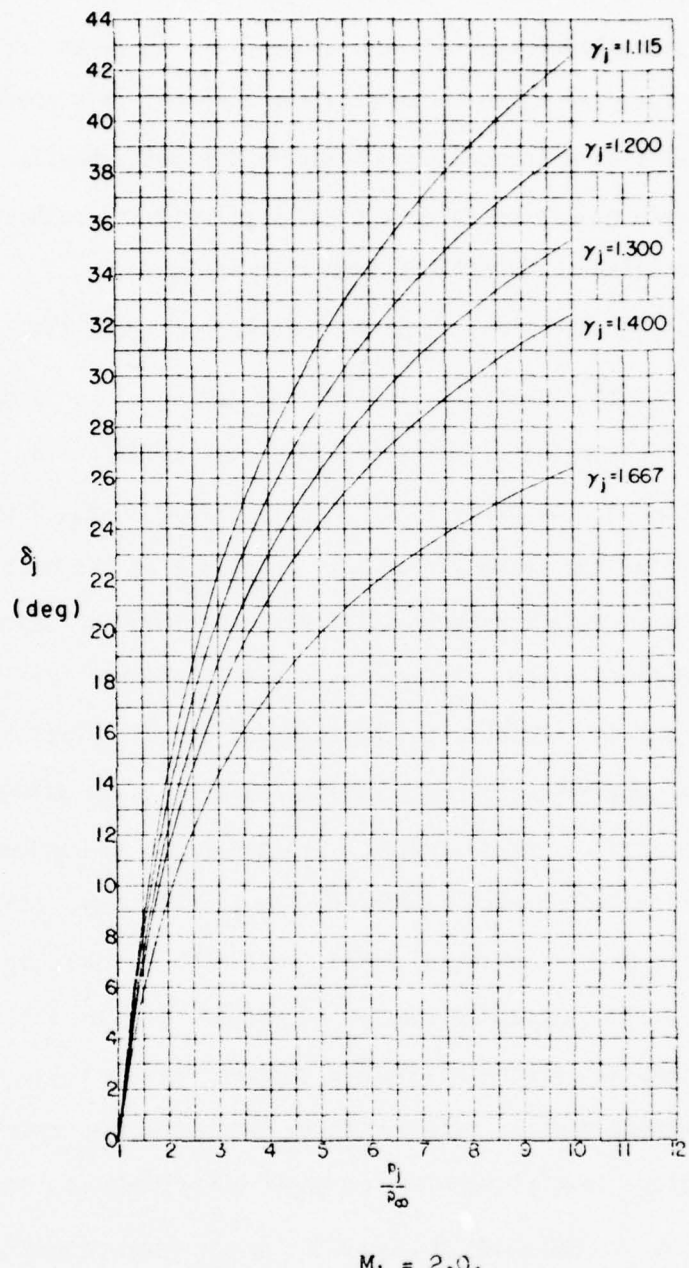


Figure 4. (Reference 4) Initial Plume Angle vs. Static Pressure Ratio

These relations are presented graphically in Figures 5 and 6.

In hot jet exhaust testing, the temperature is often varied by changing the fuel/air ratio to an ethylene burner. This produces a  $\gamma$  change as well as a temperature change in the jet exhaust. Temperature effects, therefore, can be approached as  $\gamma$  effects and both will be discussed as hot exhaust gas effects from this point on.

### 3. EFFECT OF EXHAUST PLUME $\delta_j$ ON AFTBODY NOZZLE PERFORMANCE

In an inviscid flow field, the exhaust nozzle plume is modelled as a solid body interacting with the aftbody nozzle flow field. The geometric character of the plume at the nozzle exit, i.e.  $\delta_j$ , determines the amount of turning the aftbody flow must negotiate at the nozzle exit, determines the aftbody nozzle pressure distribution, and hence the external nozzle performance. References 6 and 7 indicate the boattail drag coefficient variations with the changing exhaust plume  $\delta_j$ 's.

Figure 7 shows the effect of nozzle plume simulators on aftbody drag for a typical nozzle. As the solid plume simulator is changed from a solid cylindrical sting with a base area to a cylindrical sting with no base area to an underexpanded plume shape, the  $\delta_j$  increases and the aftend drag coefficient subsequently decreases. Each of these three solid plume simulators correspond to a nozzle pressure ratio and a  $\delta_j$  value. The aftbody drag variation with  $\delta_j$  indicates the importance of the exhaust plume initial inclination angle on aftbody performance.

### 4. CORRECTION OF COLD EXHAUST GAS DATA FOR HOT EXHAUST GAS EFFECTS

Typical advanced turbofan and turbojet engines have exhaust gas total temperatures near  $3200^{\circ}\text{R}$  in afterburning power and  $1500^{\circ}\text{R}$  in dry cruise power. Past attempts to establish  $\delta_j$  as a correlating parameter for

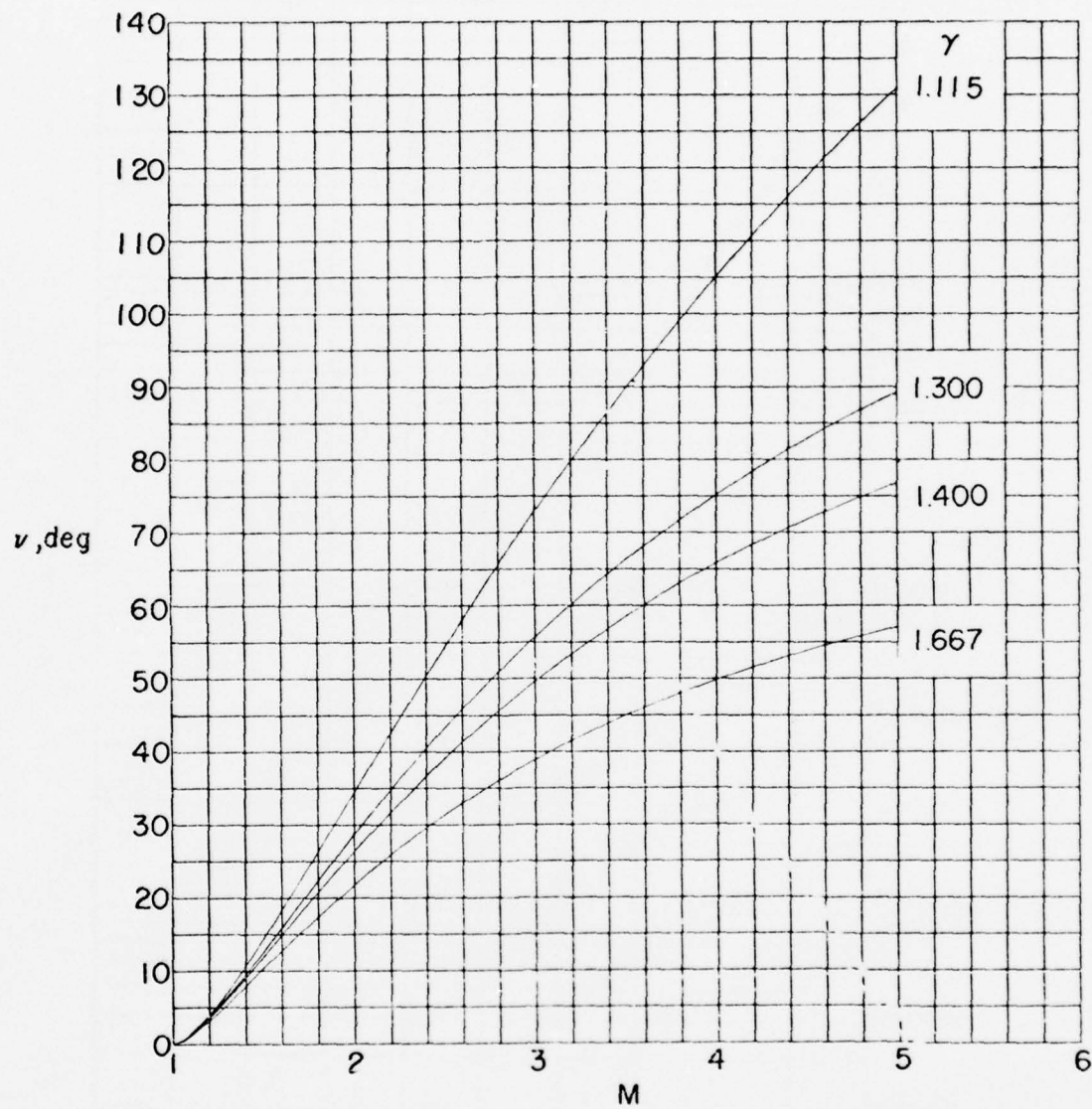


Figure 5. (Reference 5) Effect of the Ratio of Specific Heats Upon The Variation in Prandtl-Meyer Turning Angle

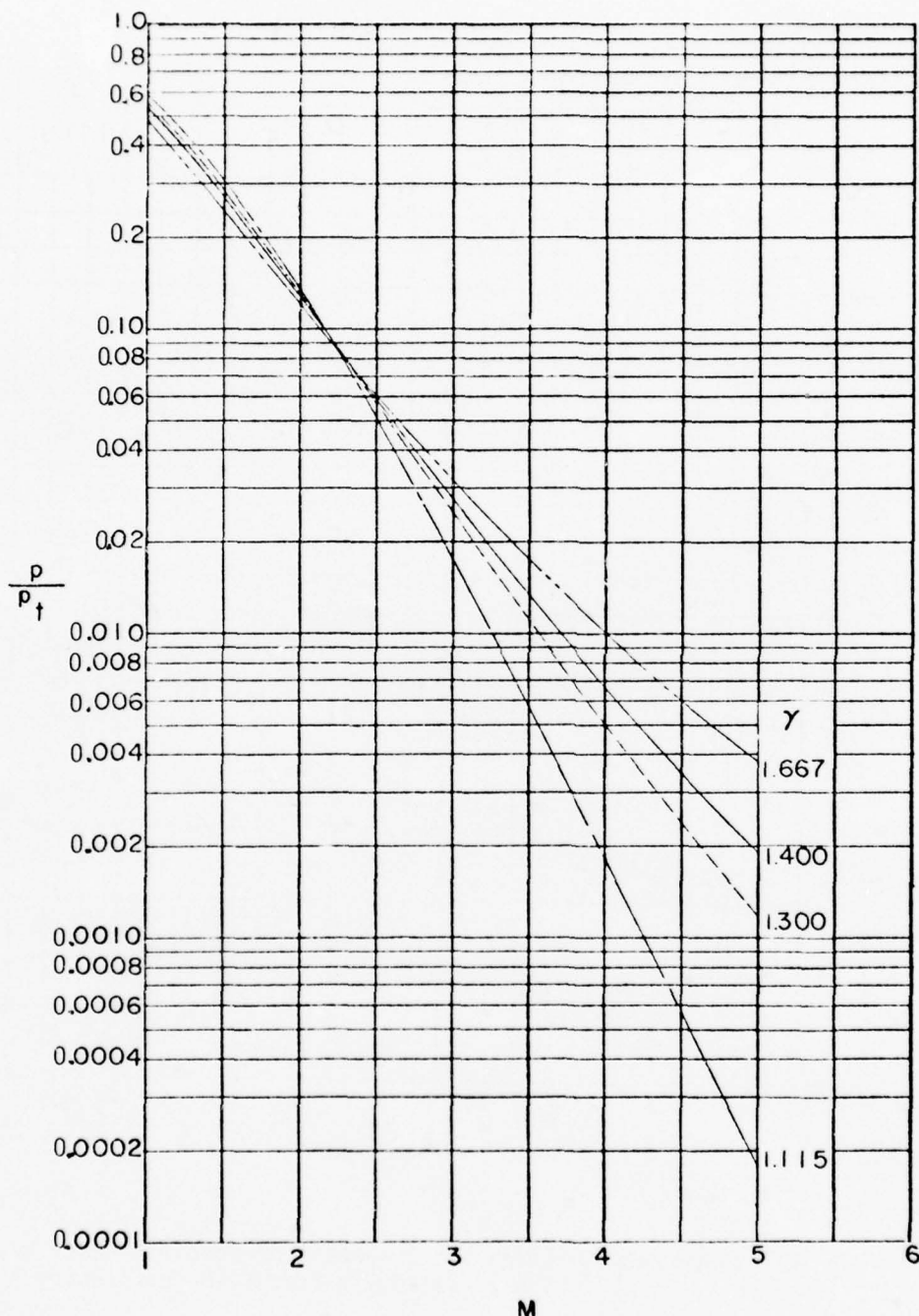


Figure 6. (Reference 5) Effect of the Ratio of Specific Heats Upon the Variation in the Ratio of Static to Stagnation Pressure with Mach Number

BEST AVAILABLE COPY

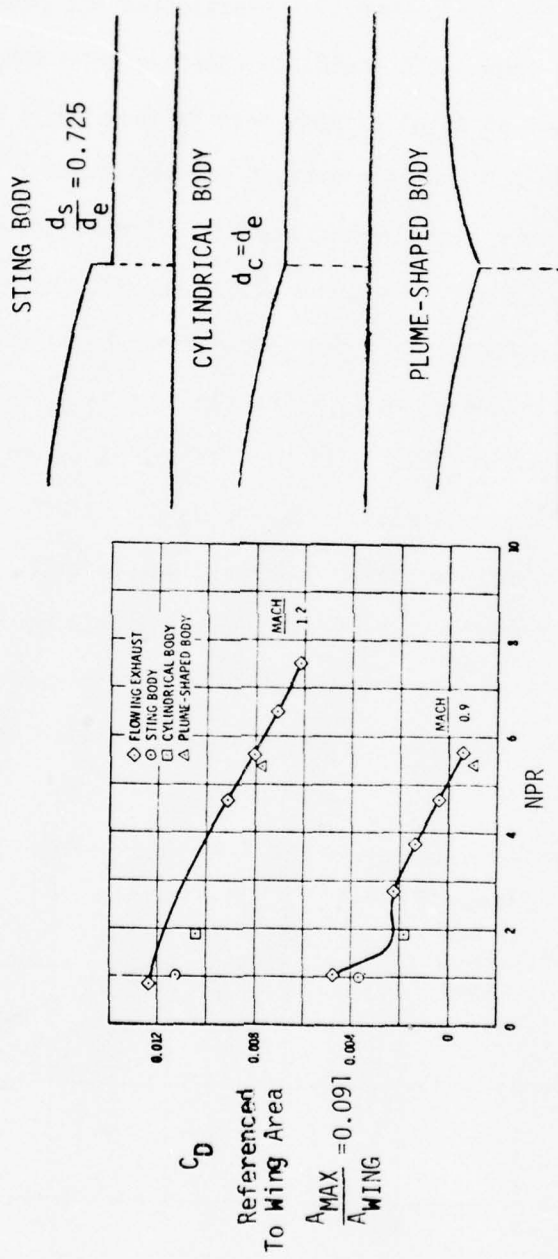


Figure 7. (Reference 7) Effect of Nozzle Plume Simulators on Aftbody Drag

hot exhaust gas effects are reported in References 1 and 2. C. E. Robinson, ARO, Inc. (Reference 1), investigated hot exhaust gas effects for temperatures from  $530^0R$  (cold) to approximately  $3200^0R$ . The effect of the hot exhaust on total aftbody drag in this study is shown in Figure 8 for  $M_\infty = 0.9$ . As the exhaust gas temperatures are increased from  $530^0R$  to  $2390^0R$ , the aftbody drag coefficient decreases. Similarly, W. Compton, NASA Langley, Figure 9 (Reference 2), shows the aftbody drag coefficient for different  $\gamma$ 's and temperatures collapsing together to an extent when correlated using  $\delta_j$ . The top plot is  $C_D$  versus  $P_T/P_\infty$  or nozzle pressure ratio (NPR). The middle plot is  $C_D$  versus static pressure ratio and the lower plot is  $C_D$  versus  $\delta_j$ . If the  $\delta_j$  correlation successfully accounts for all hot exhaust gas effects, the lower plot in Figure 9 would consist of one line, i.e., all data would collapse on all other data. It should be noted that the  $\delta_j$  correlation does not entirely compensate for hot exhaust gas effects but does tend to compress the data.

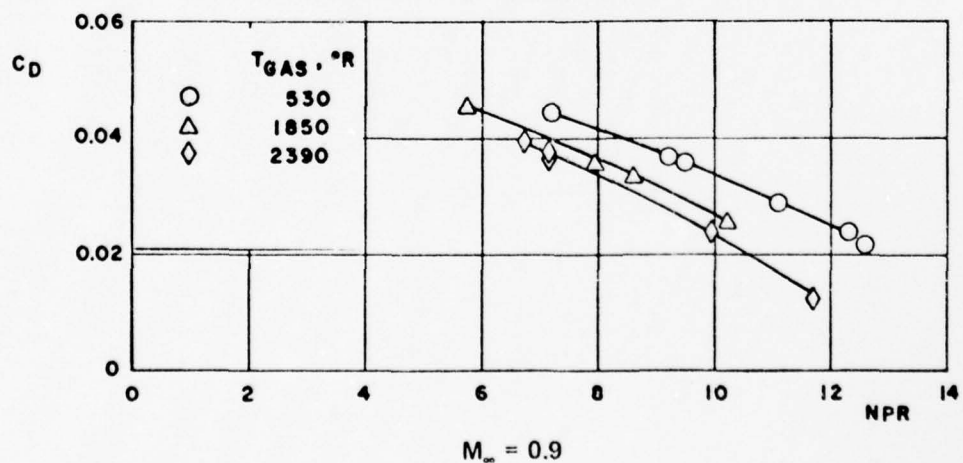


Figure 8. (Reference 1) Drag Coefficient Sensitivity with Temperature

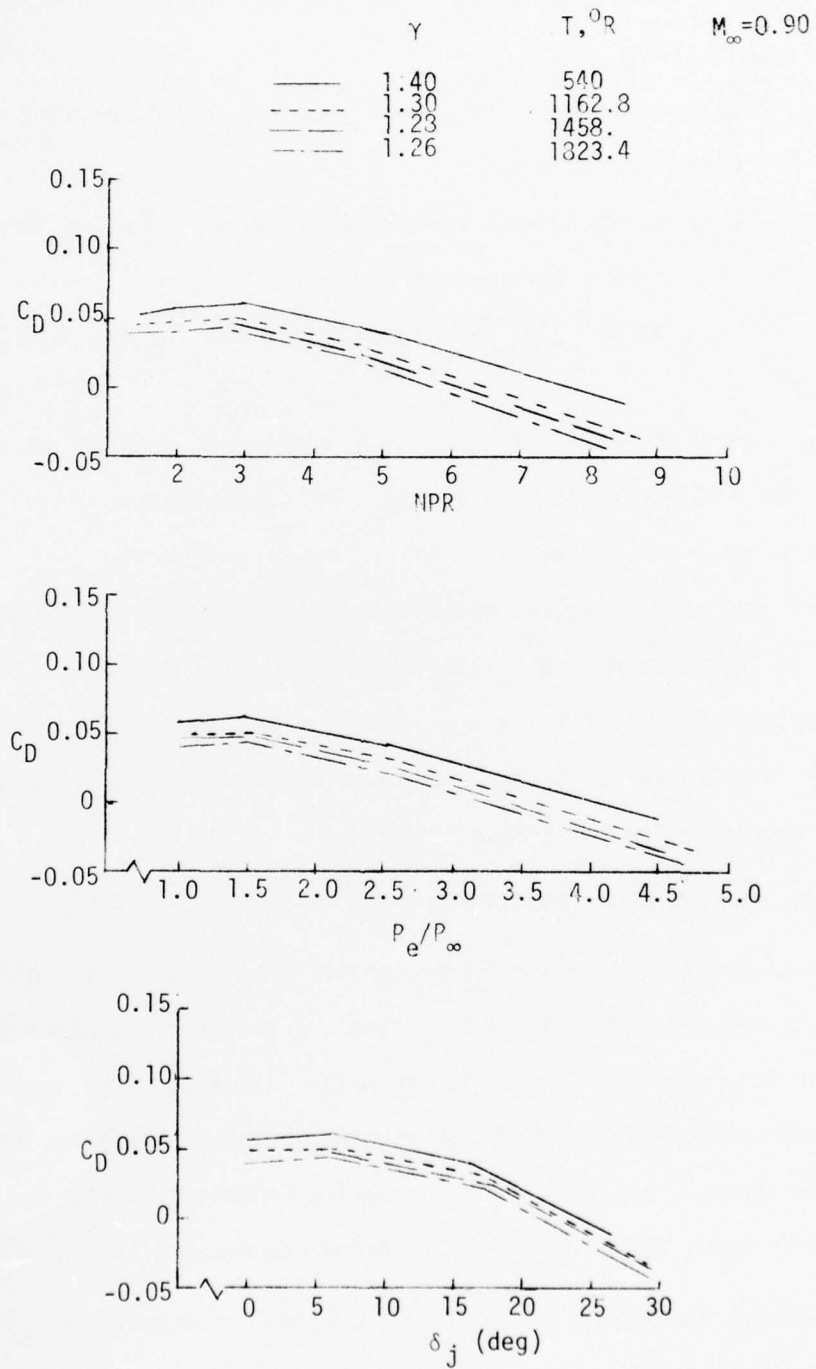


Figure 9. (Reference 2) Aftbody Drag Sensitivity

To use  $\delta_j$  as a correlating parameter, the following procedure is used. (See Figure 10).

- a. The baseline data for a cold jet, i.e.  $\gamma=1.4$  for air, is in a form  $C_D$  vs NPR (experimental data).
- b. Using the techniques discussed in the next section, a plot of  $\delta_j$  vs NPR is made as a function of  $\gamma$ .
- c. The  $\delta_j$  vs NPR plot is entered at the NPR for the data to be corrected.
- d. For a correction to  $\gamma=1.3$  i.e. a hot jet, continue up the plot until the  $\gamma=1.3$  curve is intersected. This intersection gives the  $\delta_j$  to simulate using  $\gamma=1.4$  flow.
- e. For this  $\delta_j$  value, move laterally on the plot until the  $\gamma=1.4$  curve is intersected. This intersection gives the NPR using  $\gamma=1.4$  exhaust gas that simulates a  $\gamma=1.3$  exhaust gas, i.e. simulates the same  $\delta_j$ .
- f. The  $C_D$  value at this corrected NPR value is the original drag value corrected for hot exhaust effects.

#### 5. CALCULATION OF $\delta_j$ AND CONSTRUCTION OF THE $\delta_j$ VS NPR PLOT

A computational method for  $\delta_j$  will be developed for the examples shown in Figures 2d and 3c, i.e. subsonic and supersonic external flow with an underexpanded plume. The technique described is programmed on the Hewlett-Packard 9830 computer located in the Aerodynamics and Airframe Branch, Air Force Flight Dynamics Laboratory, Wright-Patterson Air Force Base, Ohio. NACA 1135 equation numbers are listed in parenthesis.

The calculation of the initial plume angle for subsonic external flow is as follows:

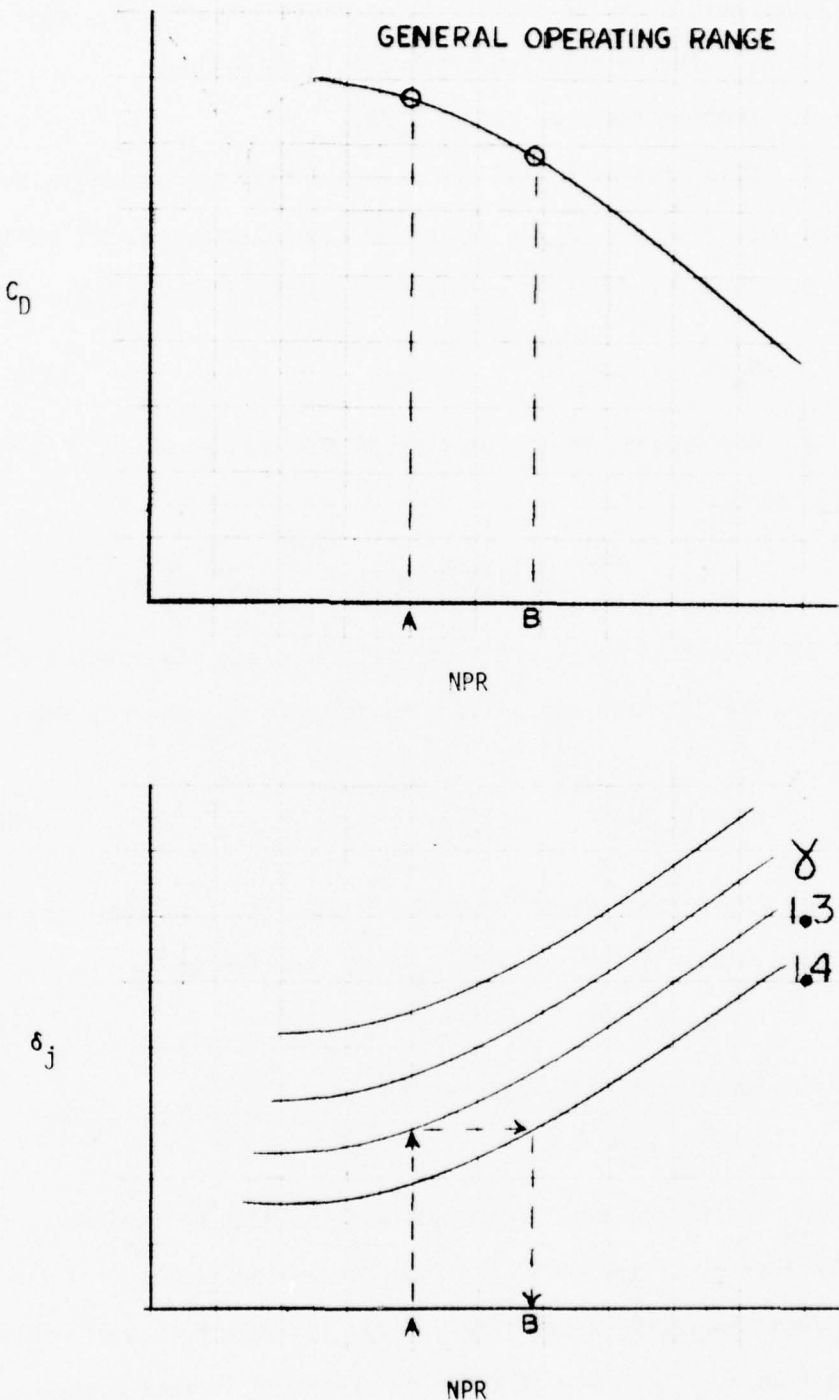


Figure 10. Drag Coefficient and Initial Plume Angle vs NPR

The known values for this calculation must be  $P_T$ ,  $A_e$ ,  $A_T$ ,  $P_{BT}$ ,  $\theta_N$ ,  $\gamma_I$ , and  $\gamma_E$ . The calculation procedure is as follows:

1. Compute the area ratio,  $A_e/A_T$
2. Using the NACA 1135 compressible flow tables, assuming  $M=1$  at the nozzle throat,  $A_e/A_*$  indicates a Mach number at the exit,  $M_e$ .
3. The exit static pressure is a function of  $P_T$ ,  $M_e$ , and  $\gamma_I$ .

$$P_e = P_T \left(1 + \frac{\gamma-1}{2} M_e^2\right)^{\frac{-\gamma}{\gamma-1}} \quad (40)$$

4. The Prandtl-Meyer function of the exit flow  $v_e$ , is a function of  $\gamma_I$  and  $M_e$ .

$$v_e = \left(\frac{\gamma+1}{\gamma-1}\right)^{1/2} \tan^{-1}\left(\left(\frac{\gamma-1}{\gamma+1}\right)(M_e^2 - 1)\right)^{1/2} - \tan^{-1}(M_e^2 - 1)^{1/2} \quad (171c)$$

5. The static pressure to be matched along the initial plume boundary is  $P_{BT}$ . The jet Mach number is a function of  $P_{BT}$  and  $P_T$ , therefore:

$$M_j = \left(\left(\frac{P_{BT}}{P_T}\right)^{\frac{\gamma-1}{\gamma}} - 1\right)^{\frac{2}{\gamma-1}} \quad (44)$$

6. The Prandtl-Meyer function in the jet, i.e. after the expansion, is determined as in step 4 with  $v_j$  as a function of  $M_j$ .

$$v_j = F(M_j, \gamma) \quad (171c)$$

7. For the Prandtl-Meyer expansion,

$$\theta_e + v_e = \theta_j + v_j$$

where  $\theta_e$  and  $\theta_j$  are flow directions with respect to the nozzle sidewall.  $\theta_e$ , therefore, is zero.  $\theta_j$  is of negative sign if the flow direction is away from the nozzle centerline. A new variable  $\theta_j^+$  is of opposite sign convention, i.e. positive if the flow direction is away from the nozzle centerline, Figure 11.

Therefore,

$$\theta_j = v_e - v_j$$

$$\theta_j^+ = v_j - v_e$$

8. To convert to  $\delta_j$ , the flow direction must be referenced to the horizontal. The correction to  $\theta_j^+$  is the nozzle divergence half angle.

$$\delta_j = \theta_j^+ + \theta_N$$

To construct the  $\delta_j$  vs. NPR plot using this technique, the nozzle throat total pressure is varied, corresponding to the experimental nozzle pressure ratio values and the subsequent  $\delta_j$  is read from the computer solution.

The supersonic external flow  $\delta_j$  calculation process involves matching the flow direction and pressure at the exit for the internal and external nozzle flow fields. The internal flow at the exit can be adjusted by either an oblique shock or a Prandtl-Meyer expansion. Since  $\delta_j$  is defined only for angles above the horizontal plane, the external flow changes are related to oblique shock solutions only. To achieve

the proper match at the exit, a plot of  $P_j$  versus  $\delta_j$  is constructed. The jet pressure,  $P_j$ , after the Prandtl-Meyer expansion, is calculated for both internal and external flows for a series of  $\delta_j$  values. The point where the internal and external flow curves cross is the point

where  $P_j$  and  $\delta_j$  are matched for the two flows. This is the correct  $\delta_j$  value for a given set of flow conditions.

For the internal flow solution, the calculation proceeds as follows:

- a. Compute the area ratio,  $A_e/A_T$ .
- b. Using compressible flow tables, assuming  $M=1$  at the nozzle throat,  $A_e/A_*$  provides an exit Mach number,  $M_e$ .
- c. The exit static pressure is a function of  $P_T$ ,  $M_e$ , and  $\gamma_I$ .

$$P_e = P_T \left(1 + \frac{\gamma-1}{2} M_e^2\right)^{\frac{2}{\gamma-1}} \quad (40)$$

- d. The oblique shock solution is started for a wedge angle equivalent to the  $\theta_N$  value. This gives a  $\delta_j$  of 0. (Figure 12).
- e. From NACA 1135, Equation 151, the static pressure ratio across the oblique shock is approximated by:

$$\begin{aligned} \frac{P_j}{P_e} = & \frac{1 + \frac{\gamma M^2 \delta}{2}}{(M^2 - 1)^{1/2}} + \frac{\gamma M^2 (\gamma + 1) M^4 - 4(M^2 - 1)}{4(M^2 - 1)^2} \delta^2 \\ & + \frac{\gamma M^2}{(M^2 - 1)^{1/2}} \left( \frac{\gamma + 1}{32} \right)^2 M^8 - \frac{7 + 12\gamma - 3\gamma^2}{24} M^6 \\ & + \frac{3}{4} (\gamma + 1) M^4 - M^2 + \frac{2}{3} \delta^3 + \dots \end{aligned} \quad (151)$$

where  $M = M_e$ ,  $\gamma = \gamma_I$ , and  $\delta$  is the angle through which the flow is turned (in radians).

- f. The jet pressure is then

$$P_j = P_e [ \dots ] \quad (151)$$

g. The flow turning angle,  $\delta$ , is decreased by 1 degree and the calculation in steps 5 and 6 repeated. This procedure continues up to and including  $\delta=0$ . At that point,  $\delta_j=\theta_N$ . To increase  $\delta_j$ , the flow must expand around the nozzle exit.

h. The Prandtl-Meyer expansion procedure is started with an expansion angle of 0 degrees. This point serves as a check for the last oblique shock point.

i. The Prandtl-Meyer function at the exit,  $v_e$ , is a function of  $\gamma_I$  and  $M_e$ .

$$v_e = \left( \frac{\gamma+1}{\gamma-1} \right)^{1/2} \tan^{-1} \left( \left( \frac{\gamma-1}{\gamma+1} \right) (M_e^2 - 1) \right)^{1/2} - \tan^{-1} (M_e^2 - 1)^{1/2} \quad (171c)$$

j. From Method of Characteristic Theory.

$$\theta_e + v_e = \theta_j + v_j$$

where  $\theta_e$  and  $\theta_j$  are flow directions with respect to the nozzle sidewall.  $\theta_e$ , therefore, is zero.  $\theta_j$  corresponds to  $\delta$ , or flow turning angle.

Therefore

$$v_j = v_e + \delta^+$$

where  $\delta^+$  is positive if the flow direction is away from the nozzle centerline.

k. The initial plume angle,  $\delta_j$ , is defined as:

$$\delta_j = \theta_N + \delta^+$$

l. The jet Mach number is a function of  $v_j$  and  $\gamma_I$ . Use compressible flow tables to get  $M_j$ .  $M_j = F(v_j, \gamma_I)$

m. The jet static pressure is a function of  $P_T$ ,  $M_j$ , and  $\gamma_I$ .

$$P_j = P_T \left[ 1 + \left( \frac{\gamma_I - 1}{2} \right) M_j^2 \right]^{\frac{\gamma_I}{\gamma_I - 1}} \quad (40)$$

n. The turning angle,  $\delta$ , is incremented by 2 degrees and steps 10 through 13 are repeated. The calculation is arbitrarily stopped when the flow has expanded through the  $\theta_N + 10$  degrees.

The external flow solution is an oblique shock computation only. For an initial plume inclination angle of 0, the flow must turn back through an angle equivalent to the external boattail angle,  $\theta_{BT}$ . The calculation is started at that point.

a. The initial turning angle,  $\delta$ , must be equivalent to  $\theta_{BT}$ , Figure 13.

$$\delta_j = 0; \delta = \theta_{BT}$$

b. As in step 5 of the internal flow oblique shock computation, Equation 151 in NACA 1135 approximates the pressure jump across the oblique shock.

$$P_j = P_{T_\infty} [ \dots (151) \dots ]$$

c. The turning angle,  $\delta$ , is incremented by one degree and the calculation is continued at step 2. The calculation is arbitrarily completed with  $\delta \approx (\theta_{BT} + 10^\circ)$ , since a pressure/deflection match has usually occurred.

From these calculations for external and internal supersonic flow, the  $P_j$  versus  $\delta_j$  plot is drawn. The intersection of the two curves gives the flow direction and pressure at the nozzle exit for the given flow conditions, NPR,  $P_{BT}$ , etc. A sample calculation, which has been verified by hand calculations, is presented in Figure 14. The  $P_j$  versus  $\delta_j$  plot in Figure 15 is a result of this sample calculation.

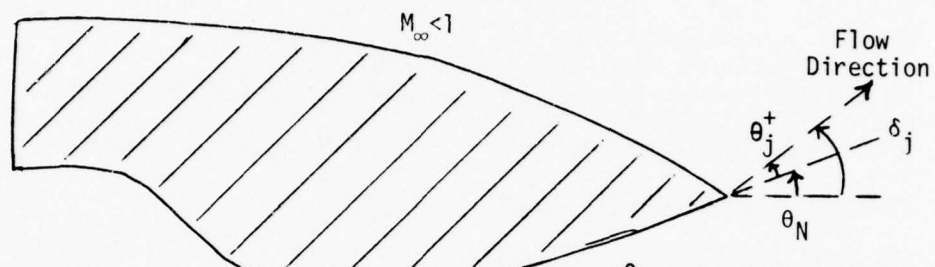


Figure 11. Nozzle Exit Flow,  $\delta_j$  Definition

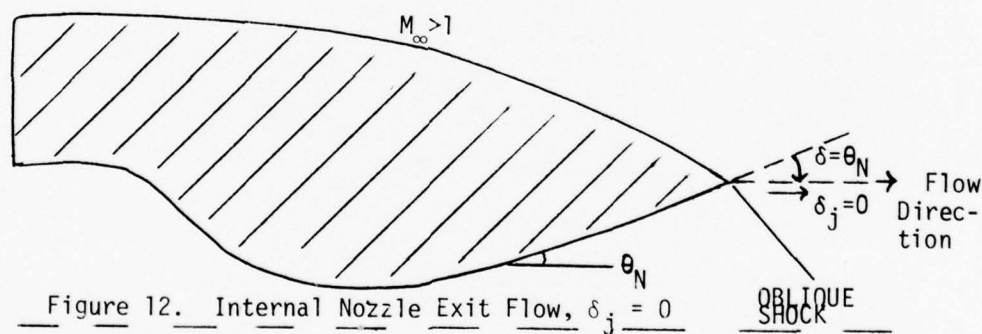


Figure 12. Internal Nozzle Exit Flow,  $\delta_j = 0$

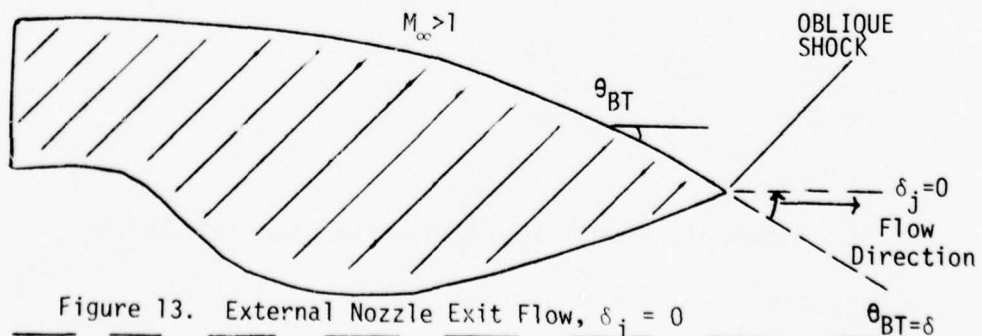


Figure 13. External Nozzle Exit Flow,  $\delta_j = 0$

# BEST AVAILABLE COPY

AFFDL-TR-76-138

SUPERSONIC EXTERNAL FLOW  
THRROAT AREA 1.0668 EXIT AREA 1.0080  
THRROAT PT,PSI 94.0000 FREESTREAM PT,PSI 125.1950  
BOATTAIL STATIC PRESSURE,PSI 16.0000  
NOZZLE DIVERGENCE HALF ANGLE,DEG 2.0000  
NOZZLE EXTERNAL BOATTAIL ANGLE,DEG 2.0000  
INT. FLOW GAMMA 1.4000 EXT. FLOW GAMMA 1.4000  
AREAR RATIO 1.0660  
AREAR RATIO 1.0660  
EXIT PRESSURE,PSI 30.3168 EXIT MACH NO. 1.3000

## INTERNAL FLOW CALCULATIONS

OBlique SHOCK CALCULATIONS  
DELTA J JET STATIC PRESSURE,PSI  
0.0000 33.5411  
1.0660 31.8736  
2.0000 30.3168

FRANDTL-MEYER EXPANSION  
FRANDTL-MEYER FCT., EXIT MACH NO. 6.1763  
DELTA J JET STATIC PRESSURE,PSI  
2.0000 30.3168  
4.0000 27.5296  
6.0000 24.9421  
8.0000 22.5524  
10.0000 20.3559  
12.0000 18.6214  
14.0000 16.7629

## EXTERNAL FLOW CALCULATIONS

BOATTAIL MACH NUMBER 2.0000  
DELTA J JET STATIC PRESSURE,PSI  
0.0000 17.8877  
1.0660 18.8953  
2.0000 19.9422  
3.0000 21.0450  
4.0000 22.1901  
5.0000 23.3839  
6.0000 24.6273  
7.0000 25.9236  
8.0000 27.2723  
9.0000 28.6757  
10.0000 30.1350

Figure 14. Sample Supersonic Freestream Calculation

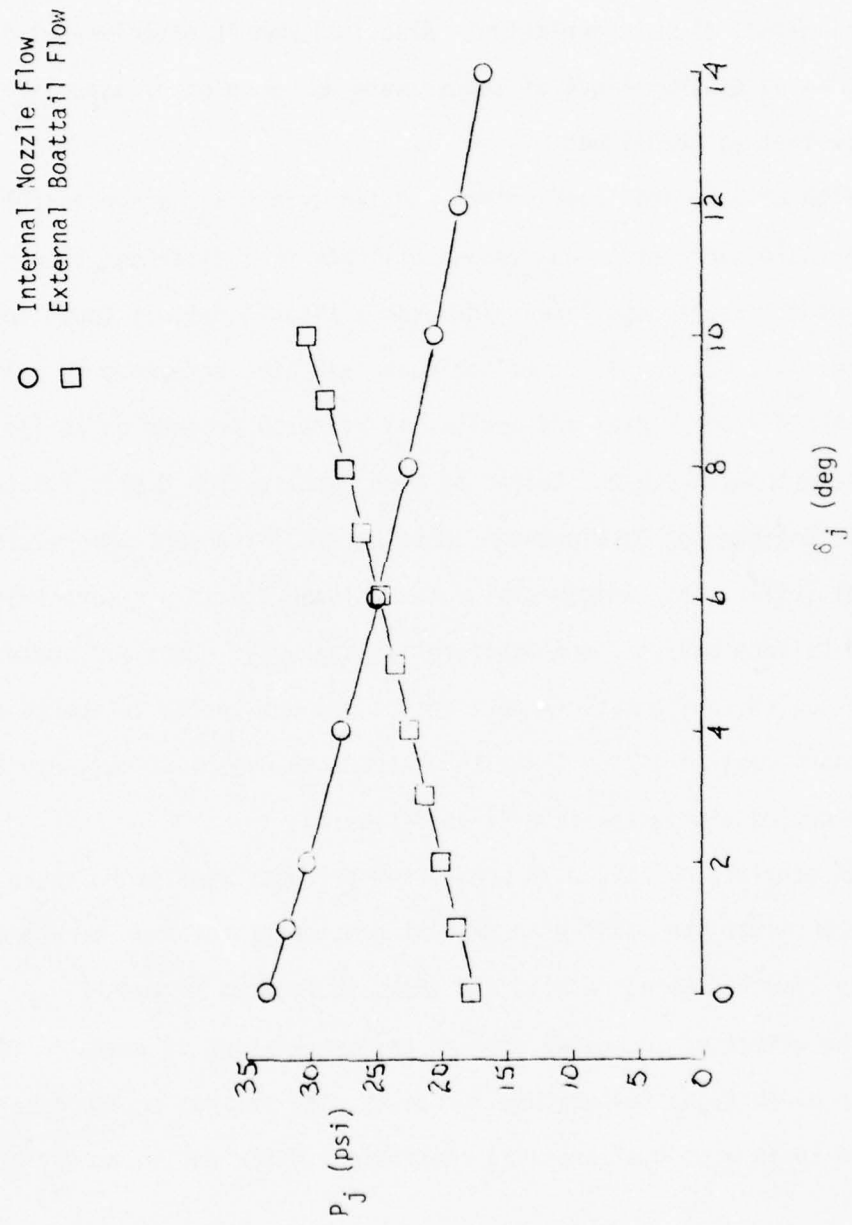


Figure 15. Pressure/Deflection Match Point

6. SURVEY OF AVAILABLE EXPERIMENTAL DATA APPLICABLE TO HOT EXHAUST GAS EFFECTS

This section contains experimental data which is directly applicable to an initial plume correlation. Also included is experimental data which assesses the effect of temperature and  $\gamma$  on other aspects of aftbody nozzle testing techniques.

With aftbody drag coefficient plotted versus  $\delta_j$ , a successful initial plume angle correlation compresses all data from different temperature exhaust gases onto one line. The best available data is found in References 1, 2, 8, and 9. C. E. Robinson, et. al., Reference 1, performed a combined experimental and analytical research program on an isolated nozzle aftbody which was tested at Mach numbers from 0.6 to 1.5 in the Arnold Engineering Development Center's (AEDC) transonic Propulsion Wind Tunnel (16T). The experimental data included static pressure orifices, force balance outputs, and Schlieren photographs. Both air-cooled and water-cooled configurations were tested but due to the influence of the secondary cooling air on the aftbody pressure distribution, only the water-cooled configuration will be discussed.

An ethylene burner, with combustion products similar to those of JP-4, provided the model with exhaust gas temperatures up to approximately  $2500^{\circ}\text{R}$ . Model details are shown in Figures 16 and 17.

The effect of increased exhaust gas temperature is shown in Figure 18. As the exhaust gas temperature increases, the aftbody nozzle drag decreases. Figure 19 is a plot of pressure coefficient distribution versus axial

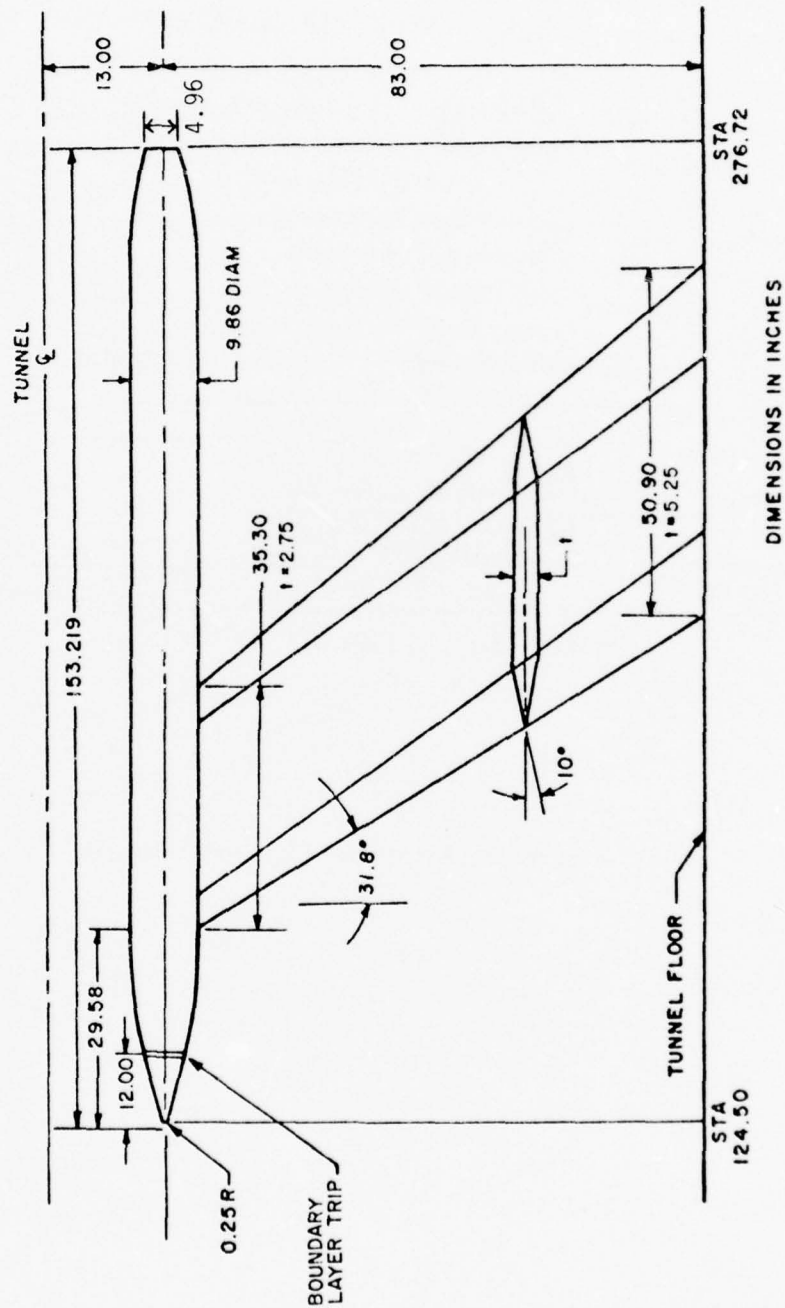


Figure 16. (Reference 1) Basic Model Dimensions and Location in Test Section

AFFDL-TR-76-138

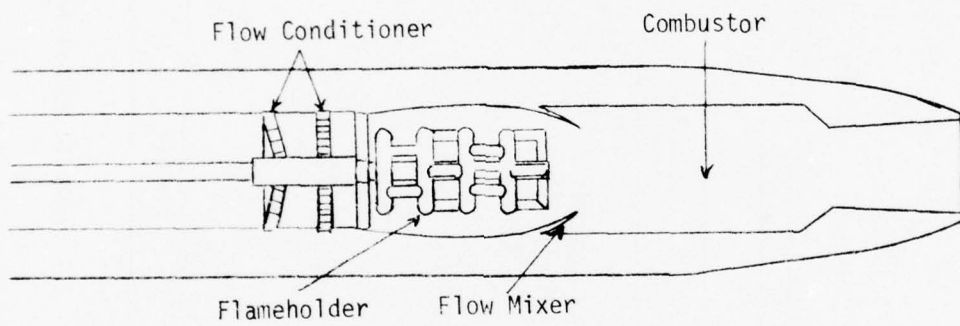
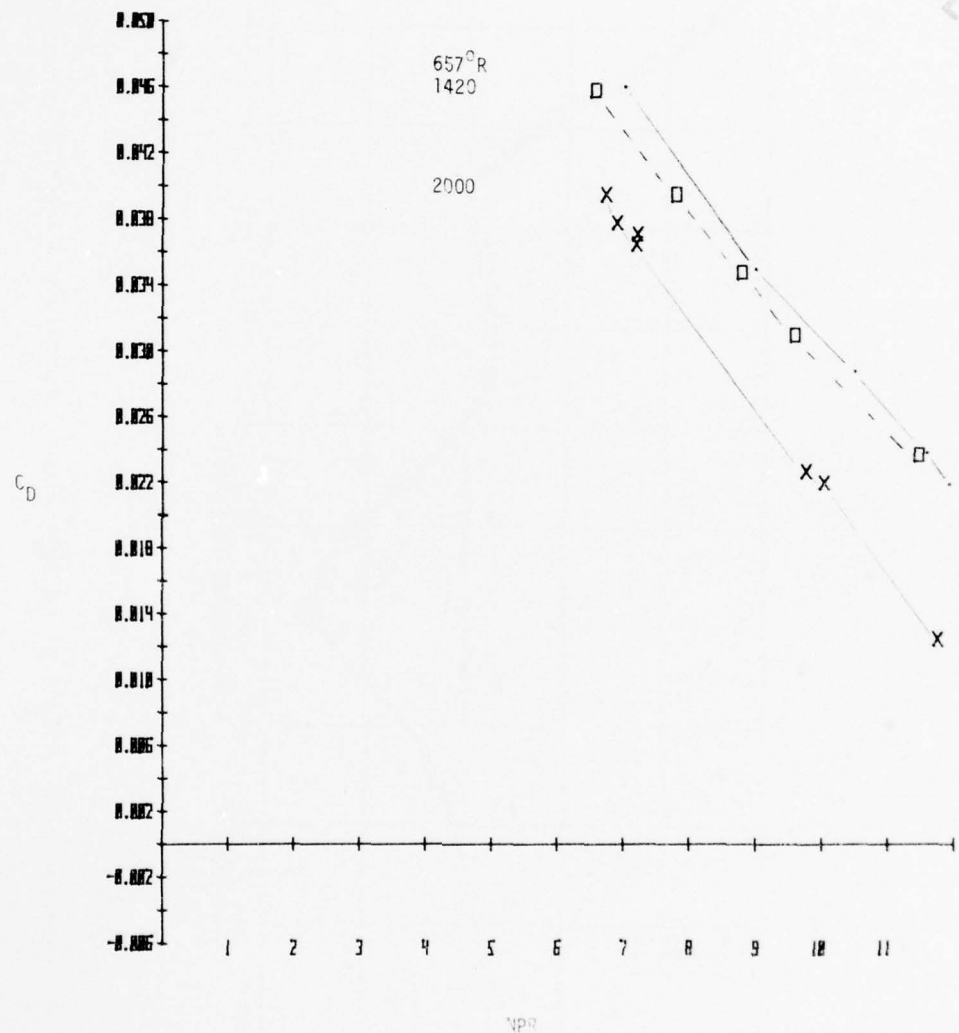


Figure 17 (Reference 1) Model Detail

Figure 18. Aftbody Pressure Drag Sensitivity with Temperature,  $M_\infty = 0.9$

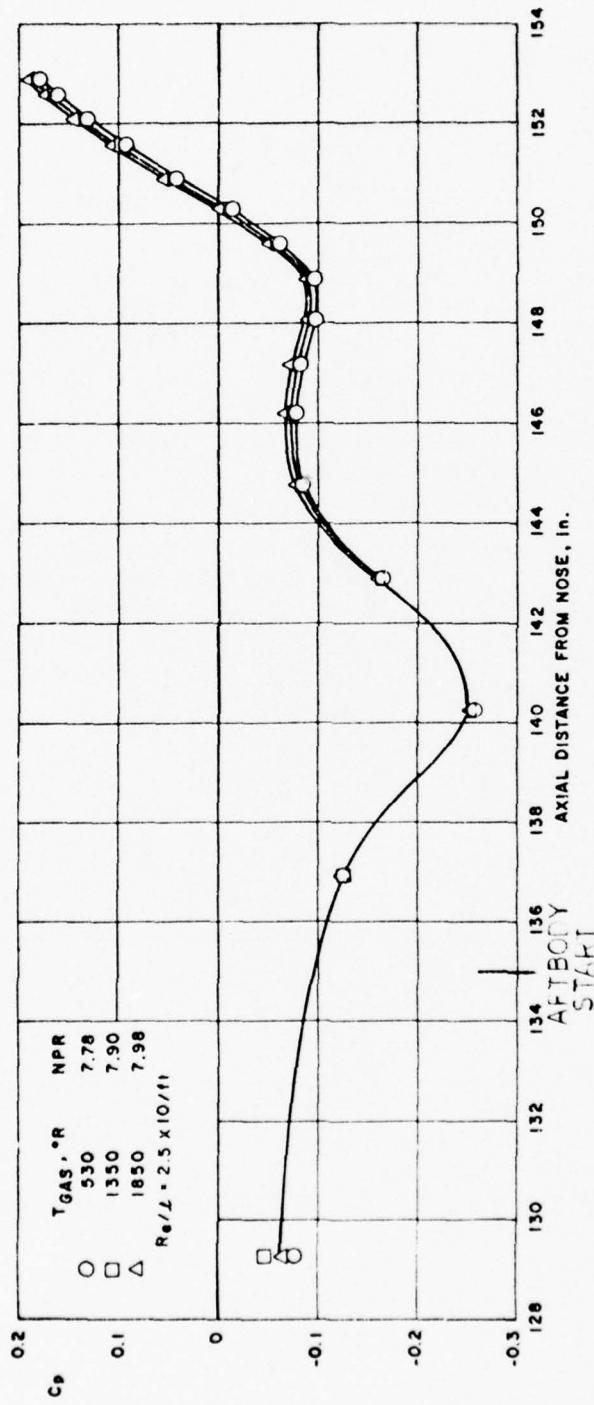


Figure 19. (Reference 1) Effect of Exhaust Plume Temperature at  $M_\infty = 0.9$

distance as a function of exhaust gas temperature. A temperature increase raises the pressure coefficient values on most of the afterbody and nozzle contours. If this change in pressure coefficient distribution can be attributed to a change in the initial plume angle the data should collapse onto one line when aftbody drag coefficient is plotted versus  $\delta_j$ . This correlation is shown in Figure 20. The correlation does tend to draw the data together, but still does not compensate for the  $2000^0R$  case and tends to over-correct the  $1420^0R$  data at higher nozzle pressure ratios.

At a freestream Mach number of 1.5, the effect of exhaust gas temperature is small (Figure 21). When the drag coefficient data is plotted versus the initial plume angle, the effect of the hot exhaust gas is over-corrected for the middle range temperatures (Figure 22).

Additional hot jet data from the Arnold Engineering Development Center's 16T facility is described in Reference 9. The test apparatus (Figure 16) is identical to that used by Robinson (Reference 1) with the exception of the nozzle boattail contours. These aftbody boattails, designated the  $15^0$  and  $25^0$  AGARD boattails, were tested by other NATO countries under the AGARD program "Improved Nozzle Testing Techniques in Transonic Flow". Efforts of other NATO countries will be discussed in additional paragraphs of this report.

Using the initial plume angles calculated by AEDC, the measured aftbody drag coefficients are plotted versus nozzle pressure ratio and initial plume angle in Figures 23 through 27. The figures include aftbody drag coefficients versus nozzle pressure ratio and initial plume inclination angle for the  $15^0$  AGARD boattail at Mach numbers of 0.8, 0.9, and 1.1. In all cases, an increase of exhaust gas temperature resulted

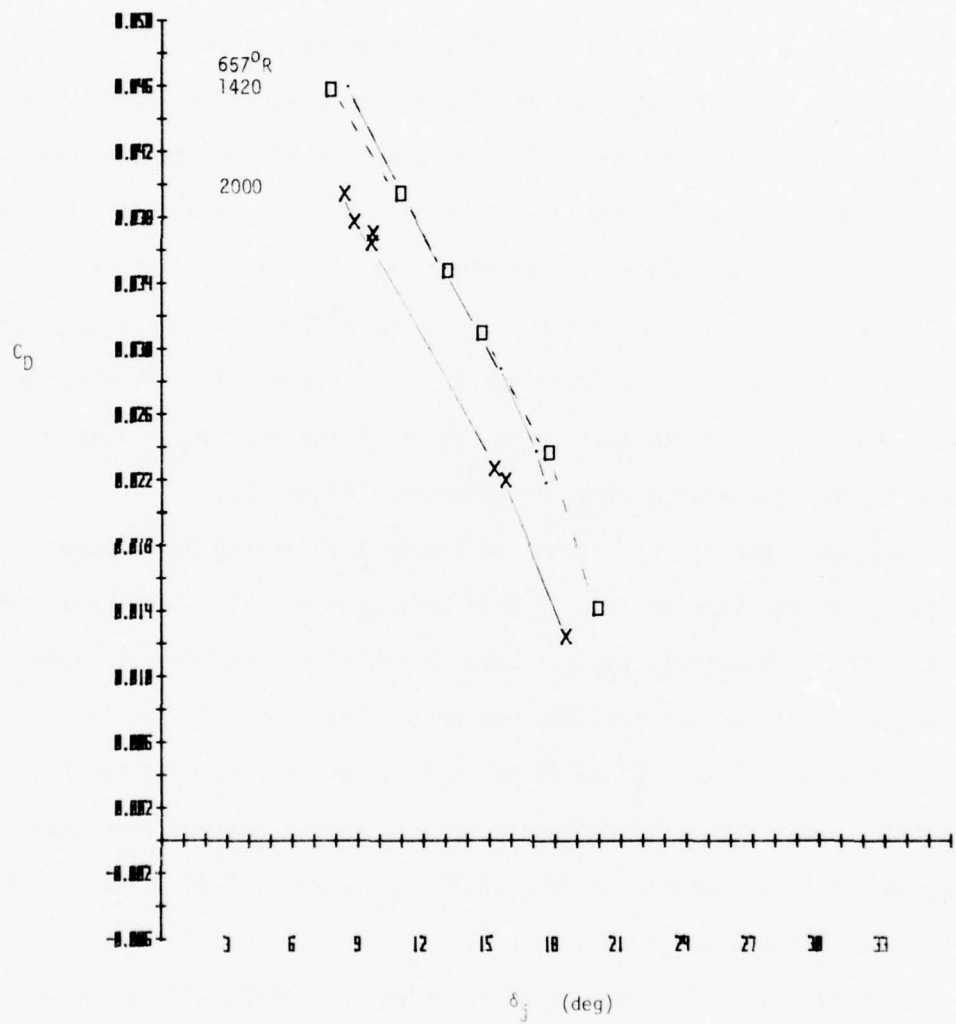


Figure 20. Initial Plume Angle Correlation, Reference 1 Data,  $M_{\infty}=0.9$

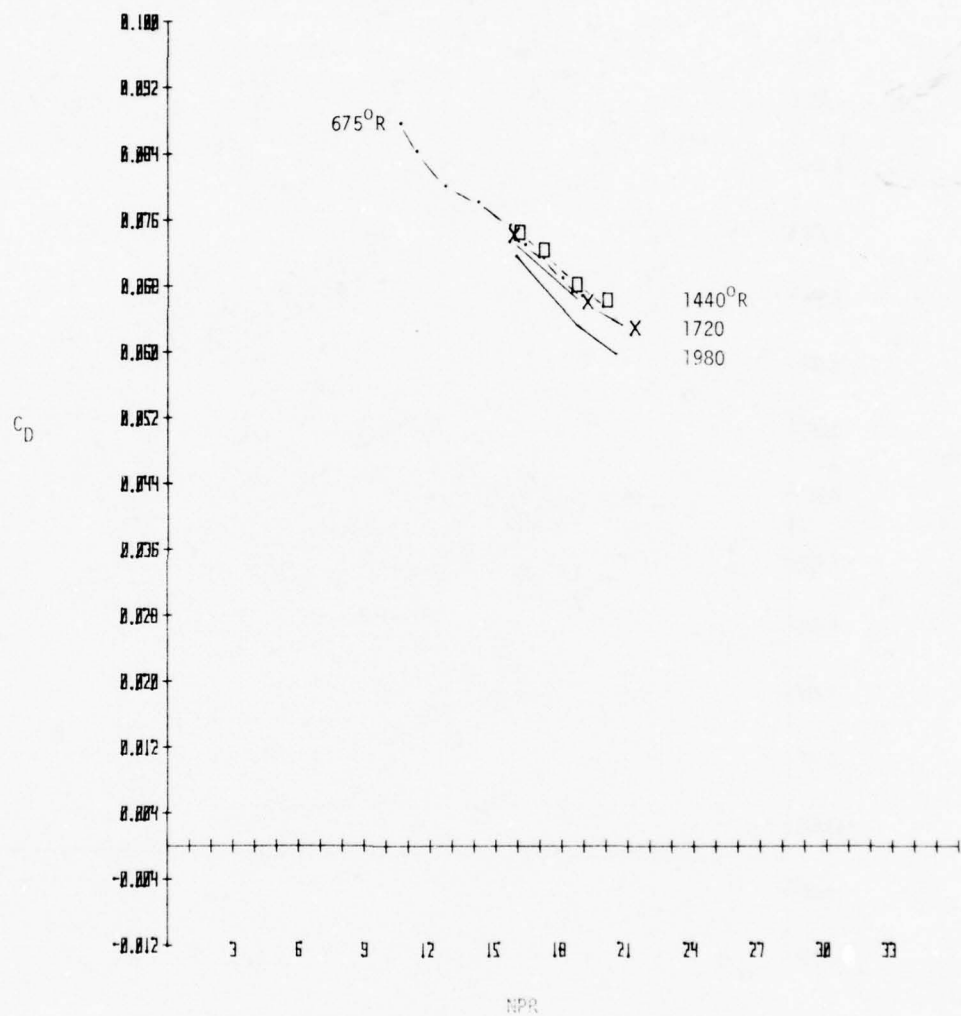


Figure 21. Drag Coefficient vs. NPR, Reference 1 Data,  $M_{\infty} = 1.5$

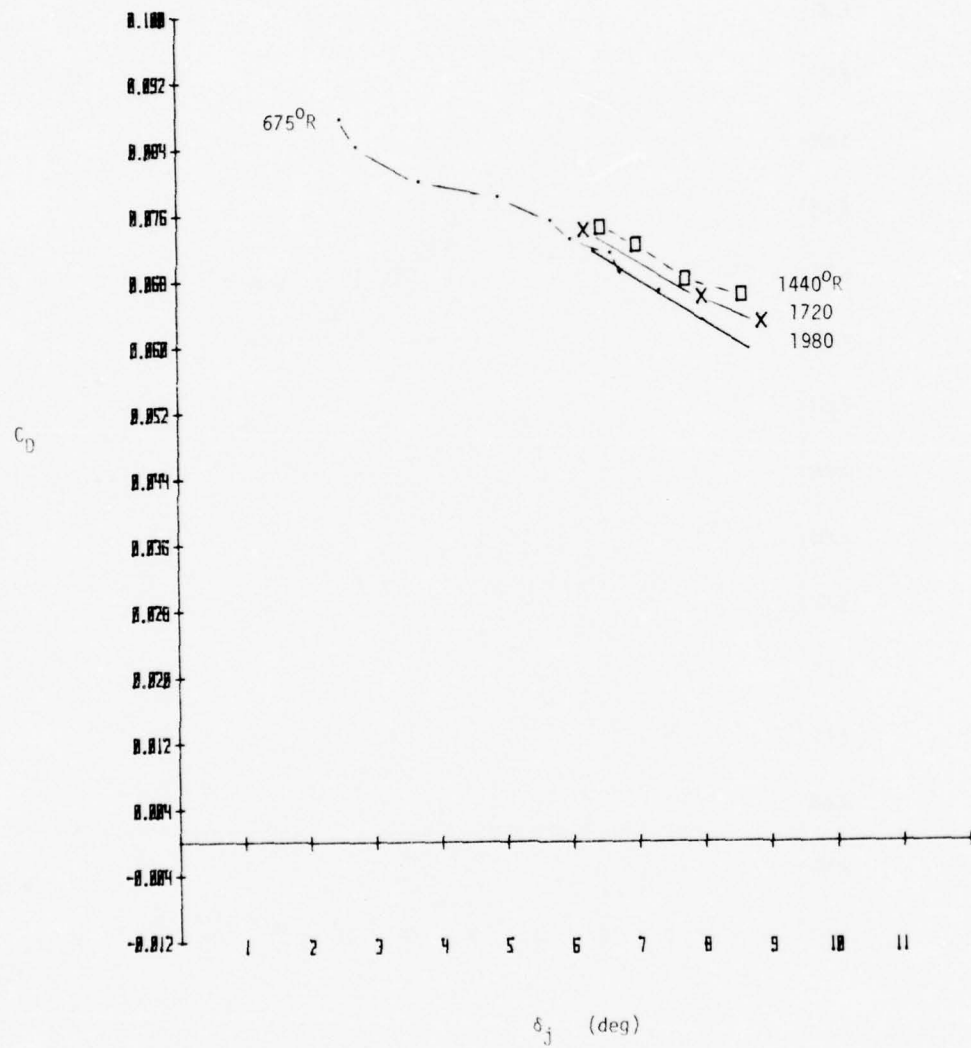


Figure 22. Initial Plume Angle Correlation, Reference 1 Data,  $M_\infty = 1.5$

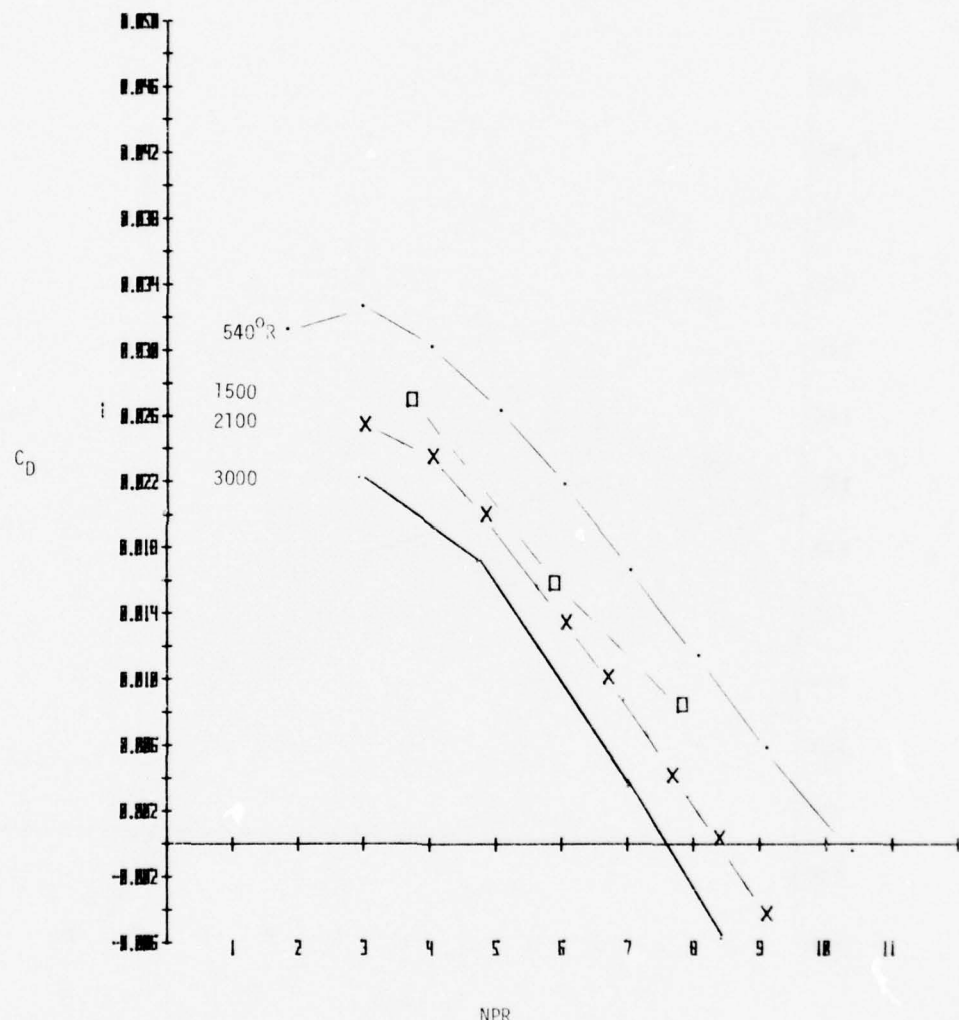


Figure 23. Drag Coefficient vs. NPR and Initial Plume Angle Correlation, Reference 9 Data,  $15^{\circ}$  Boattail,  $M_{\infty}=0.8$

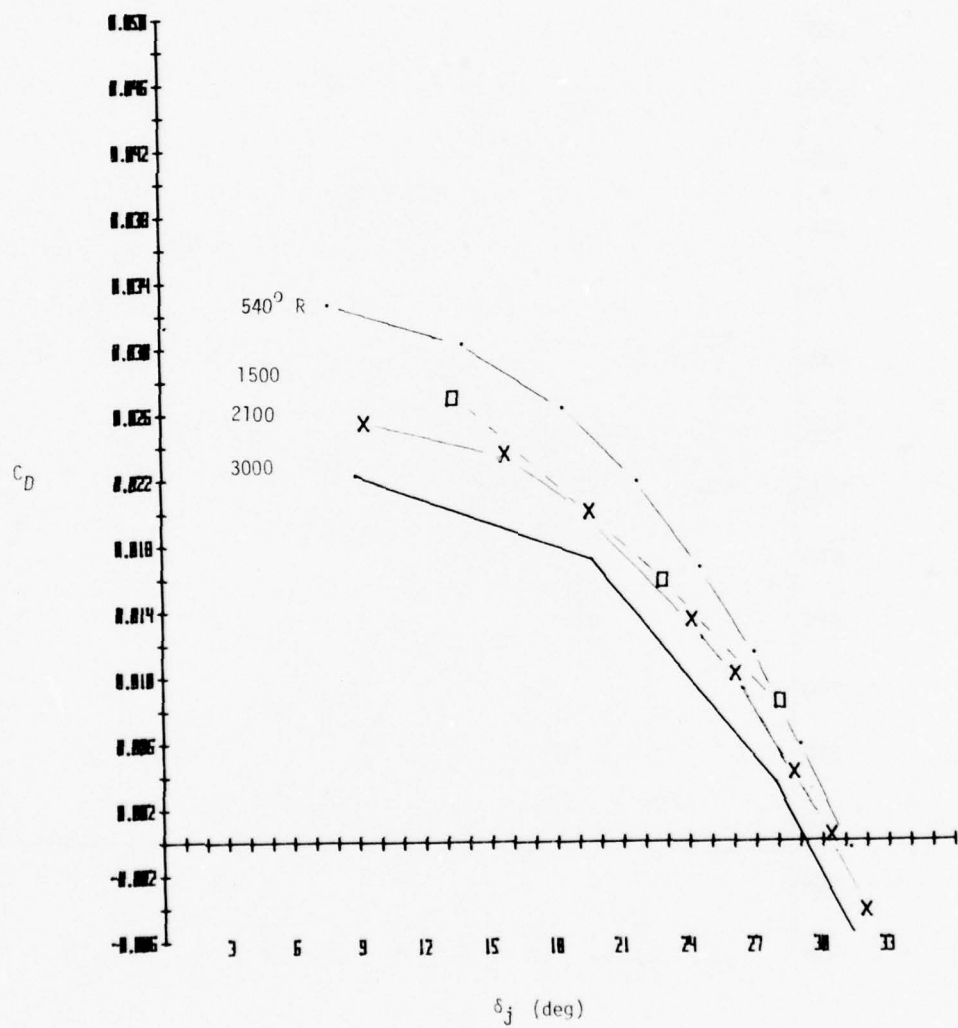


Figure 23. (Concluded)

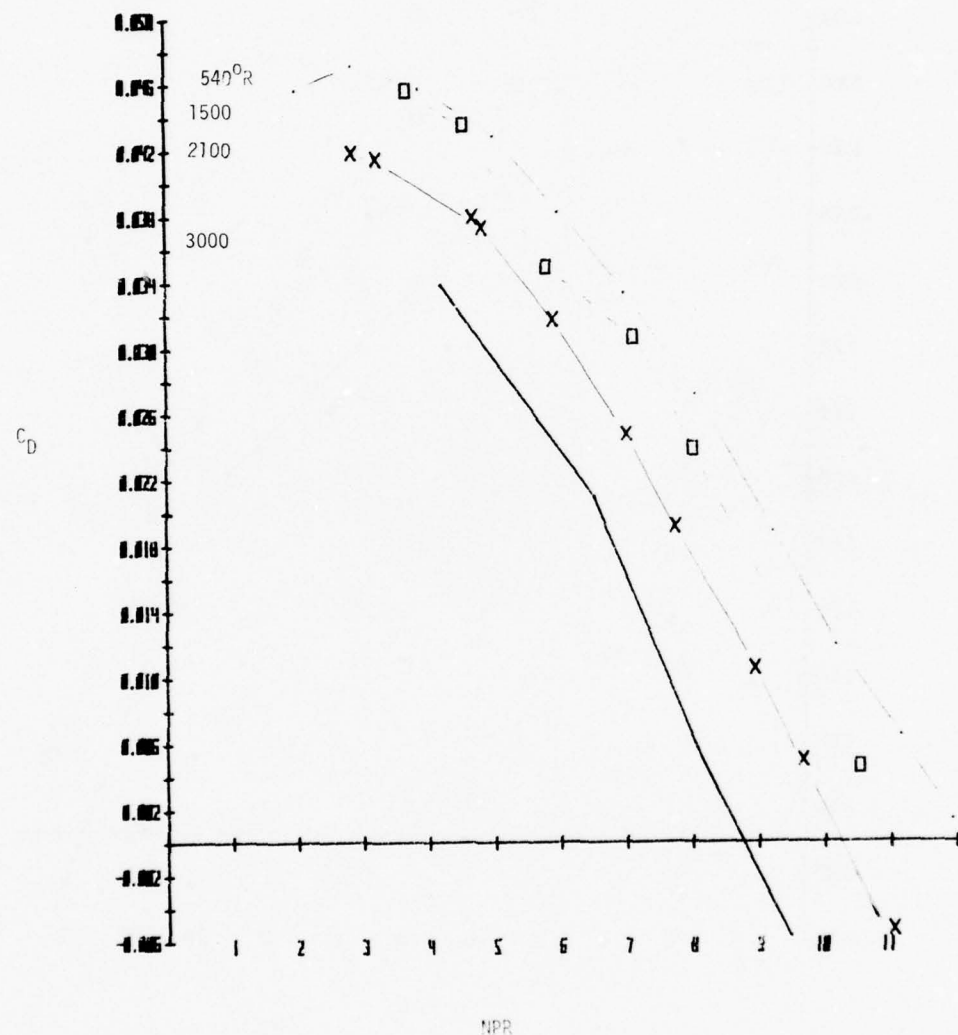


Figure 24. Drag Coefficient vs. NPR and Initial Plume Angle  
Correlation Reference 9 Data,  $15^{\circ}$  Boattail,  $M_{\infty} = 0.9$

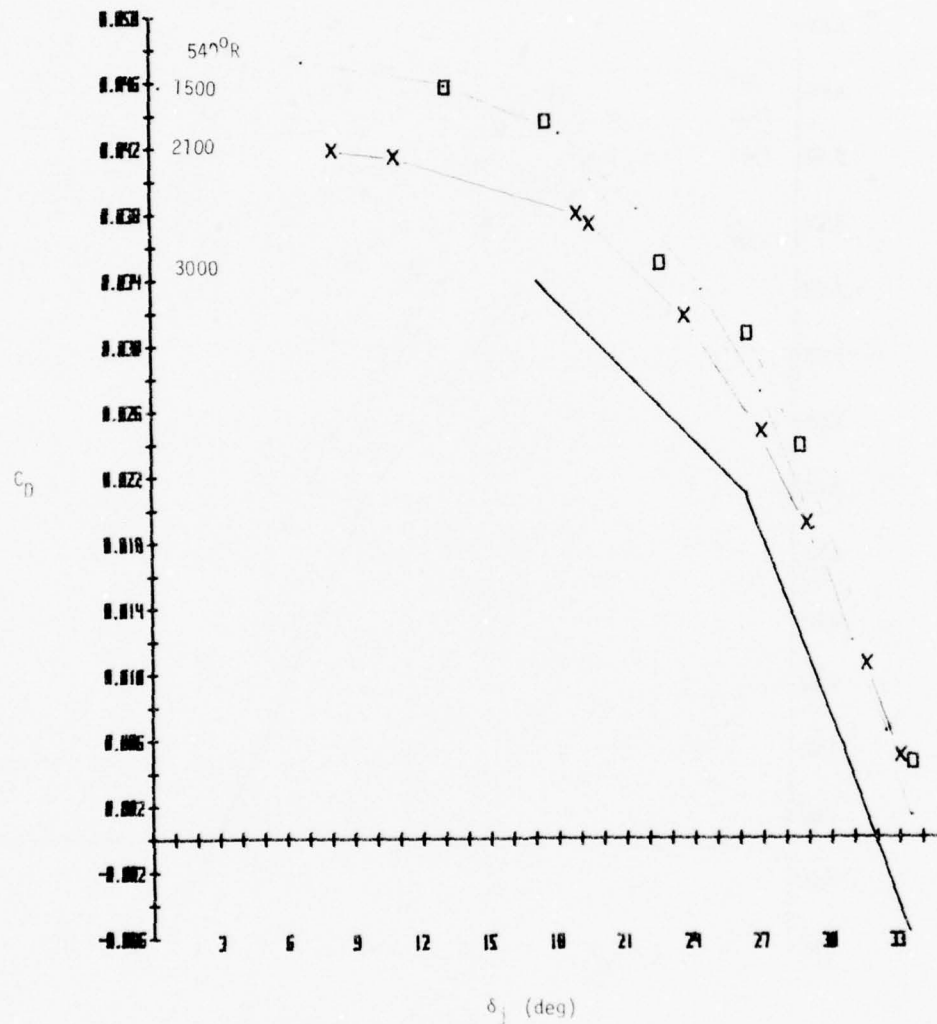


Figure 24. (Concluded)

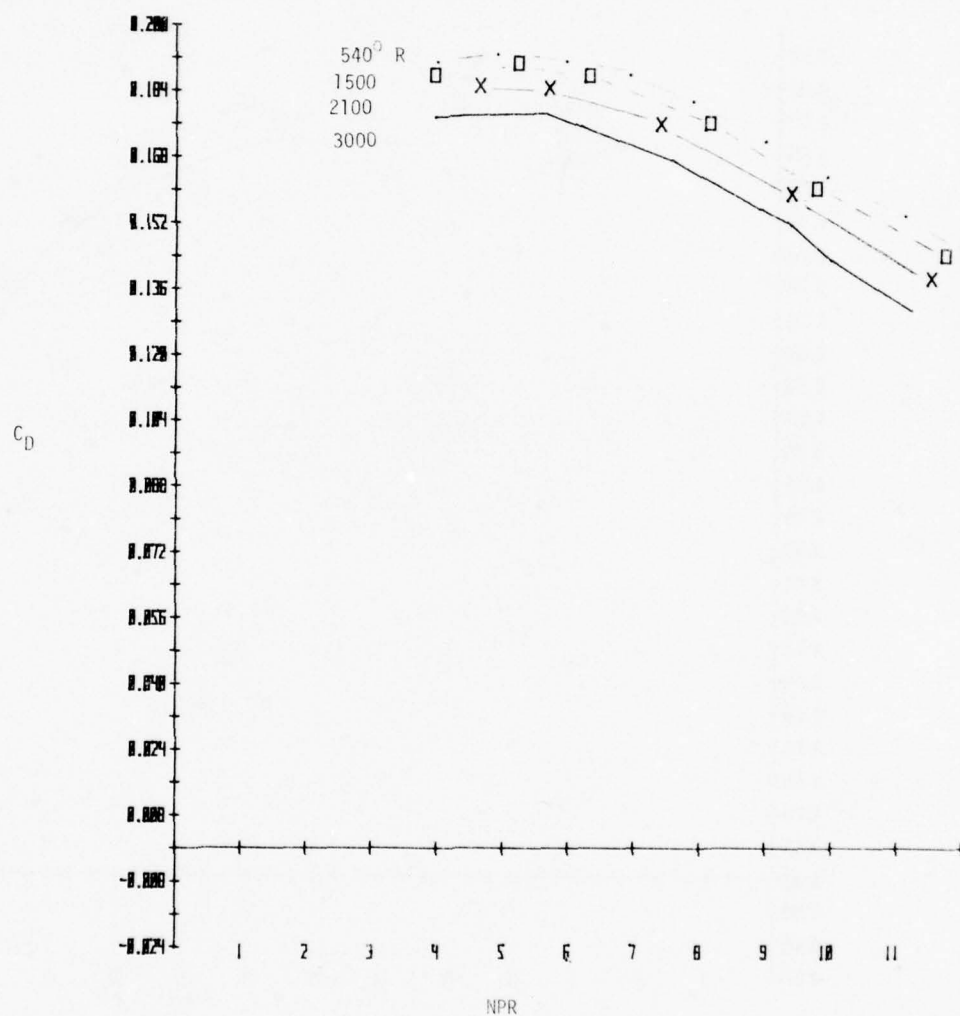


Figure 25. Drag Coefficient vs. NPR and Initial Plume Angle Correlation, Reference 9 Data, 15° Boattail,  $M_\infty = 1.1$

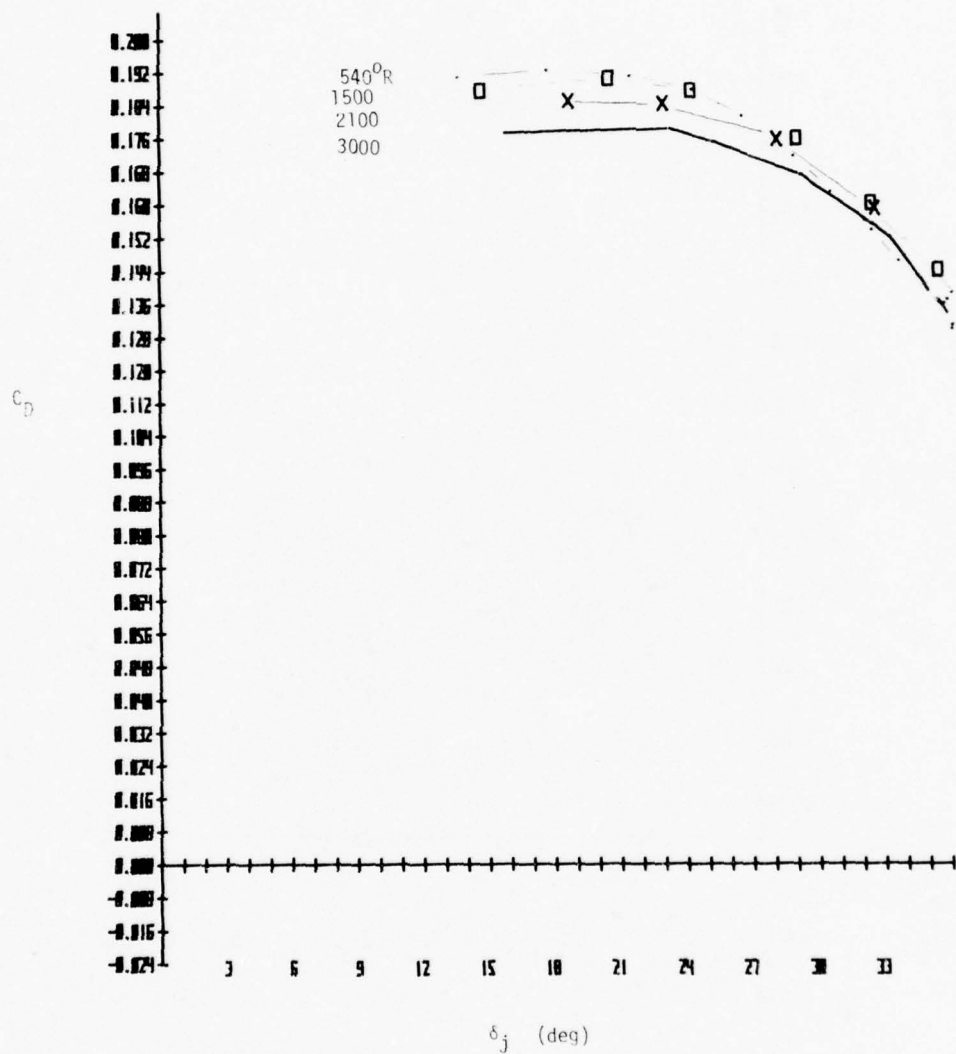


Figure 25. (Concluded)

in a decrease in aftbody drag. The exhaust gas temperatures listed are nominal values. When the drag coefficient is plotted versus the initial plume angle, the plots of different temperatures tend to collapse on one another, especially at the higher values of  $\delta_j$ , corresponding to the higher nozzle pressure ratios. At low values of  $\delta_j$ , the correlation does not appear to be effective. It should be noted that the operating nozzle pressure ratios of current turbofan and turbojet engines in the cruise conditions is 3 to 6. At this area of interest, therefore, the  $\delta_j$  correlation is not sufficient to handle hot exhaust effects.

Figures 26 and 27 present drag coefficient data for the 25° AGARD boattail. This configuration has a region of highly separated flow from the boattail shoulder aft to the exit. The aftbody drag coefficient, therefore, is relatively insensitive to nozzle pressure ratio changes. When the drag coefficient is plotted versus initial plume angle, the data spread due to hot exhaust gas effects is unchanged. This data plus the low nozzle pressure ratio data from the 15° AGARD boattail indicates that areas where the drag coefficient is marginally influenced by nozzle pressure ratio are areas where the initial plume angle correlation is ineffective.

The aftbody drag trends and the applicability of the initial plume angle correlation to a hot exhaust jet are substantiated by Reference 2. W. B. Compton, using an isolated nacelle with cold air or hydrogen peroxide exhaust jets, investigated the magnitude of the effect of various jet parameters on external nozzle boattail performance.

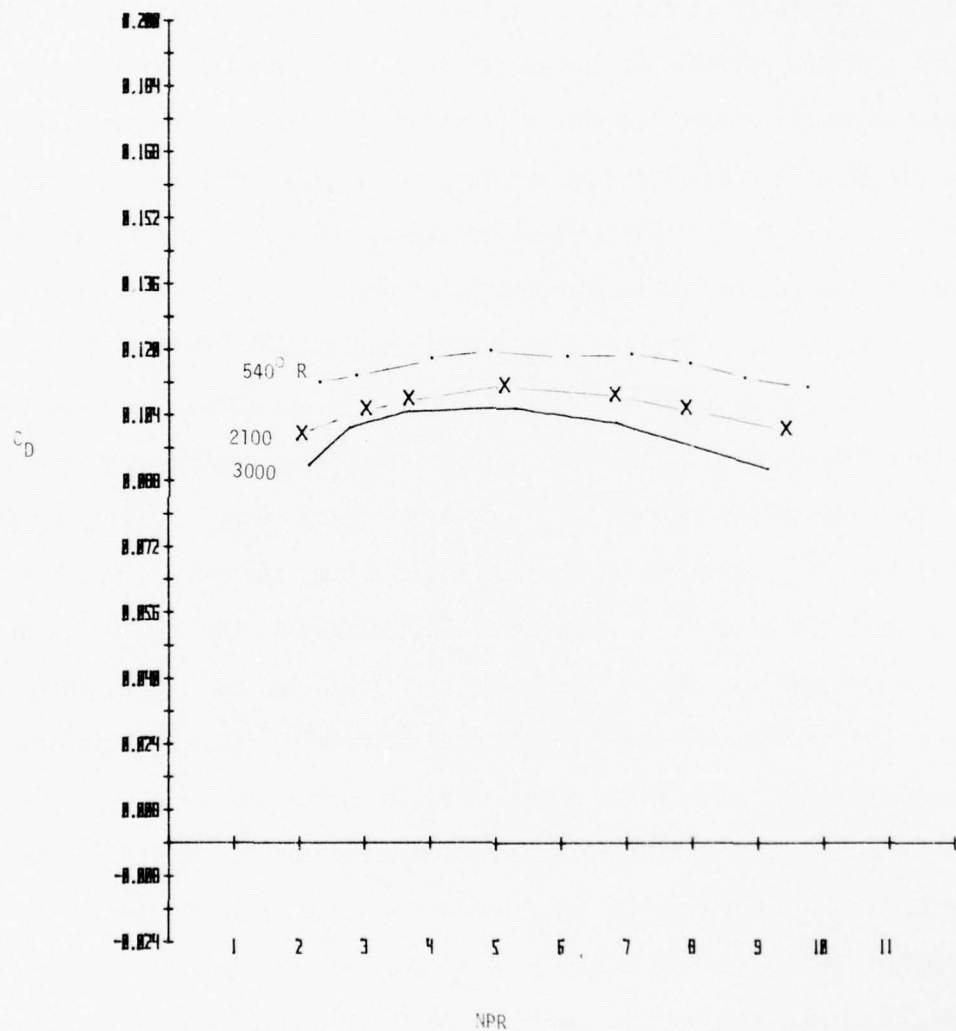


Figure 26. Drag Coefficient vs. NPR and Initial Plume Angle Correlation, Reference 9 Data, 25° Boattail,  $M_\infty = 0.8$

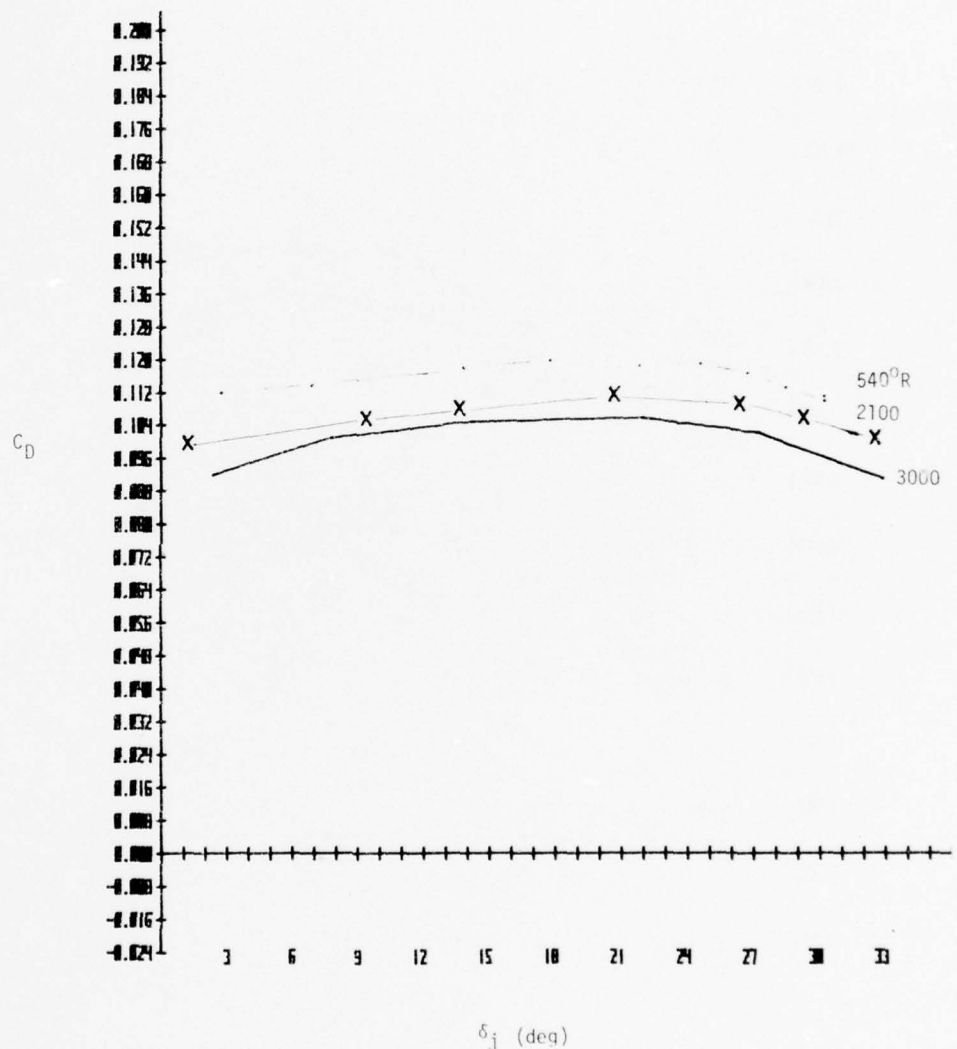


Figure 26. (Concluded)

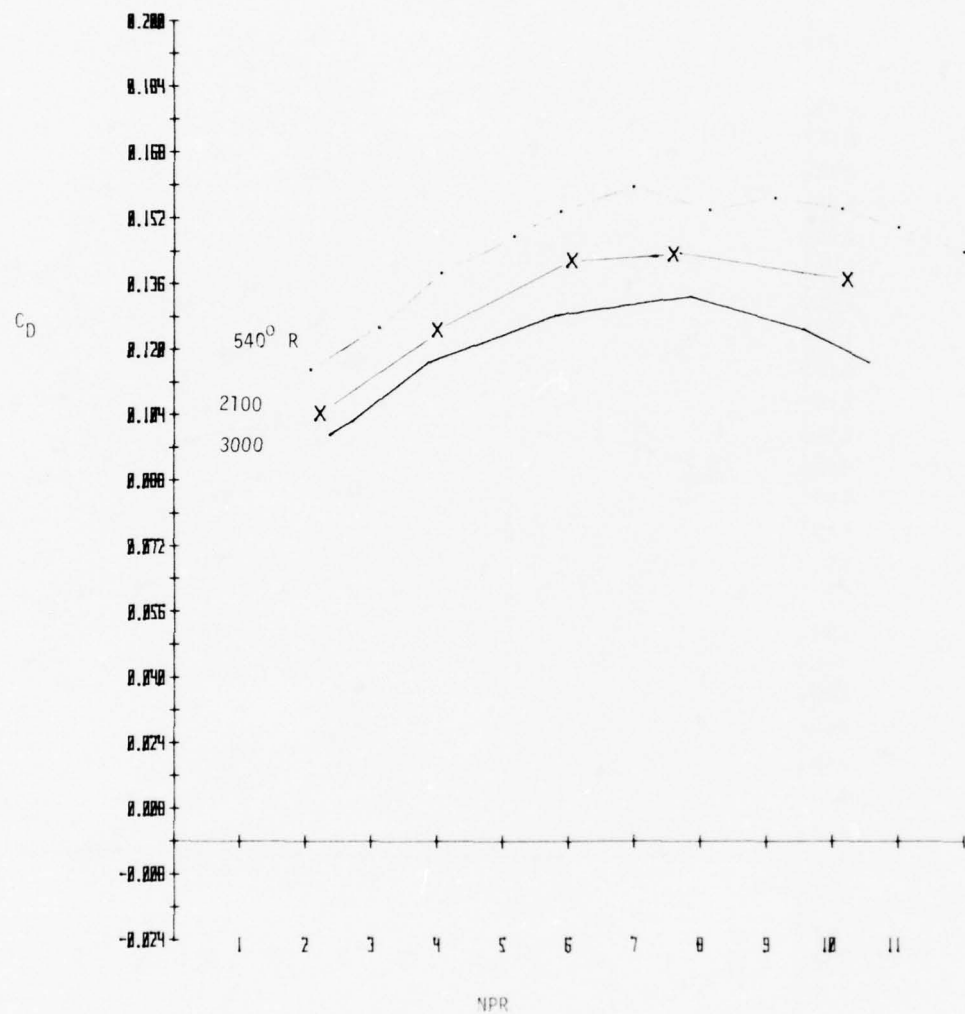


Figure 27. Drag Coefficient vs. NPR and Initial Plume Angle Correlation, Reference 9 Data, 25° Boattail,  $M_\infty = 0.9$

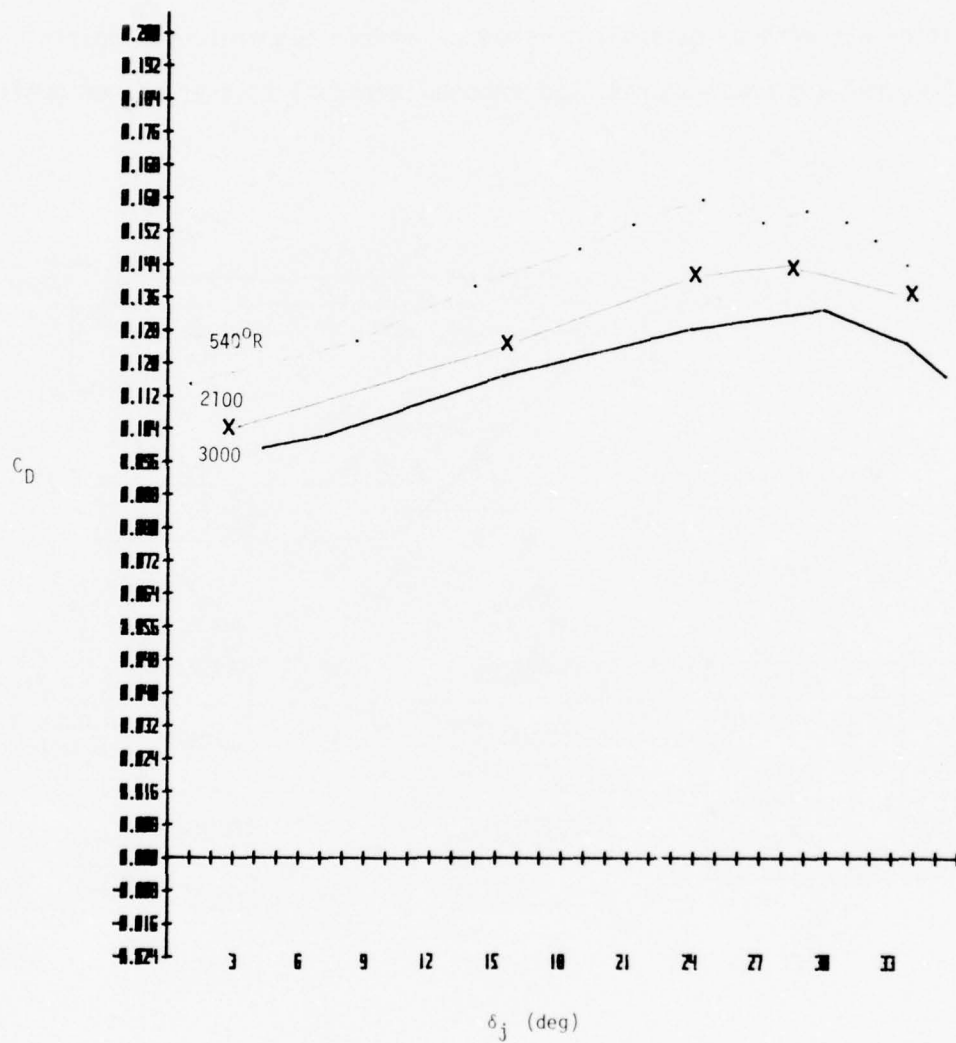


Figure 27. (Concluded)

The test apparatus and nozzle configurations are shown in Figure 28. Two nozzles with external boattail angles of  $10^\circ$  and  $20^\circ$  were tested with design internal area ratios to provide  $M_e = 1$  and  $M_e = 2$ . Primary instrumentation was aftbody external pressures, surface temperatures, nozzle exit pressures and temperatures, and external boattail boundary layer profiles.

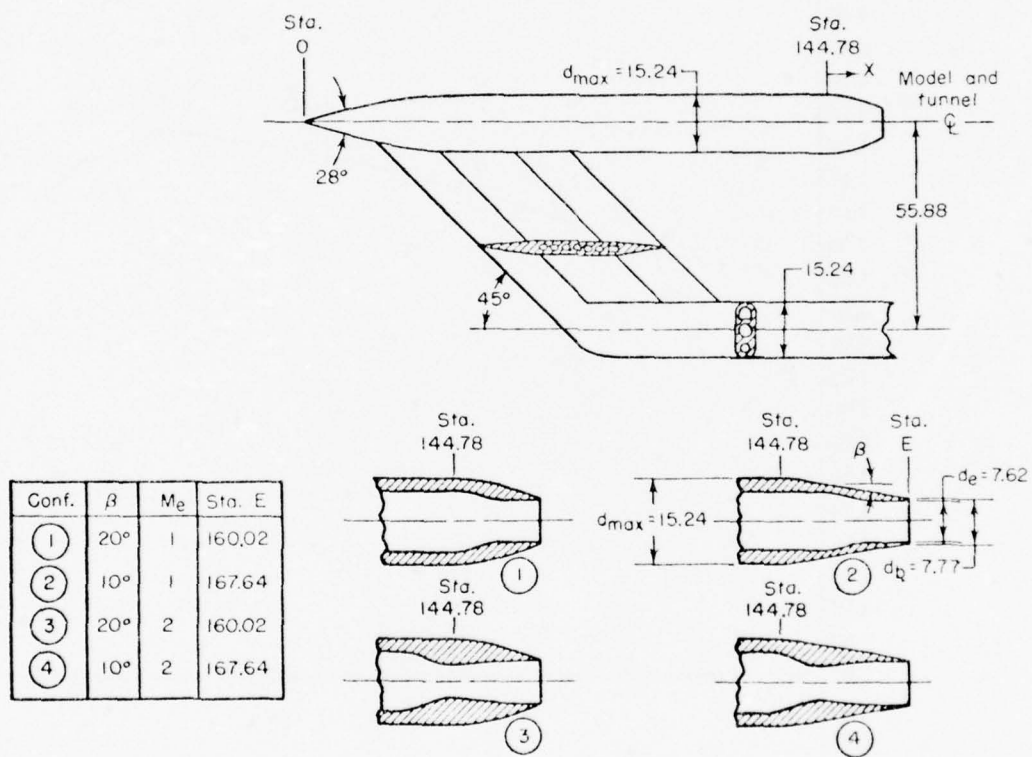


Figure 28. (Reference 2) Nozzle Details

As the exhaust gas temperature increased, the aftbody nozzle pressure distribution was altered to generally give higher pressures. Figure 29 shows this trend for a freestream Mach number of 0.9. This altered pressure distribution produces the reduced nozzle drag coefficient. One of the results of this investigation is that the greatest drag differences for varying exhaust gas temperature occurred for high transonic Mach numbers ( $M \approx 0.95$ ) and large external boattail angles ( $\theta_{BT} = 20^\circ$ ). A correlation of the drag coefficient and the initial plume angle is shown in Figures 30 and 31 for freestream Mach numbers of 0.9 and 1.2, respectively. The correlation tends to collapse the drag coefficient data together, especially at large values of nozzle pressure ratio. This trend is consistent with previous work. Compton attributed the remaining spread in drag coefficient data to jet entrainment.

Tests conducted by the NACA on simple convergent nozzles demonstrated the effects of a hot exhaust jet on afterbody nozzle drag. The transonic tests were conducted in the Langley 8-foot transonic wind tunnel with nacelle contours of varying boattail angles (Figure 32). Exhaust jet temperatures of 540°R, 1260°R, and 1660°R were provided by an ethylene burner. Primary instrumentation was external aftbody static pressures.

Using the computer coding for subsonic external flow, the initial plume angle correlation was computed at Mach numbers of 0.8 and 0.9. Plots of total aftbody drag coefficient versus nozzle pressure ratio (NPR) and initial plume inclination angle ( $\delta_j$ ) are presented in Figures 33 and 34 for Mach numbers of 0.8 and 0.9, respectively. For aftbody boattail configurations with relatively low boattail angles, i.e. 16 and 24 degrees,

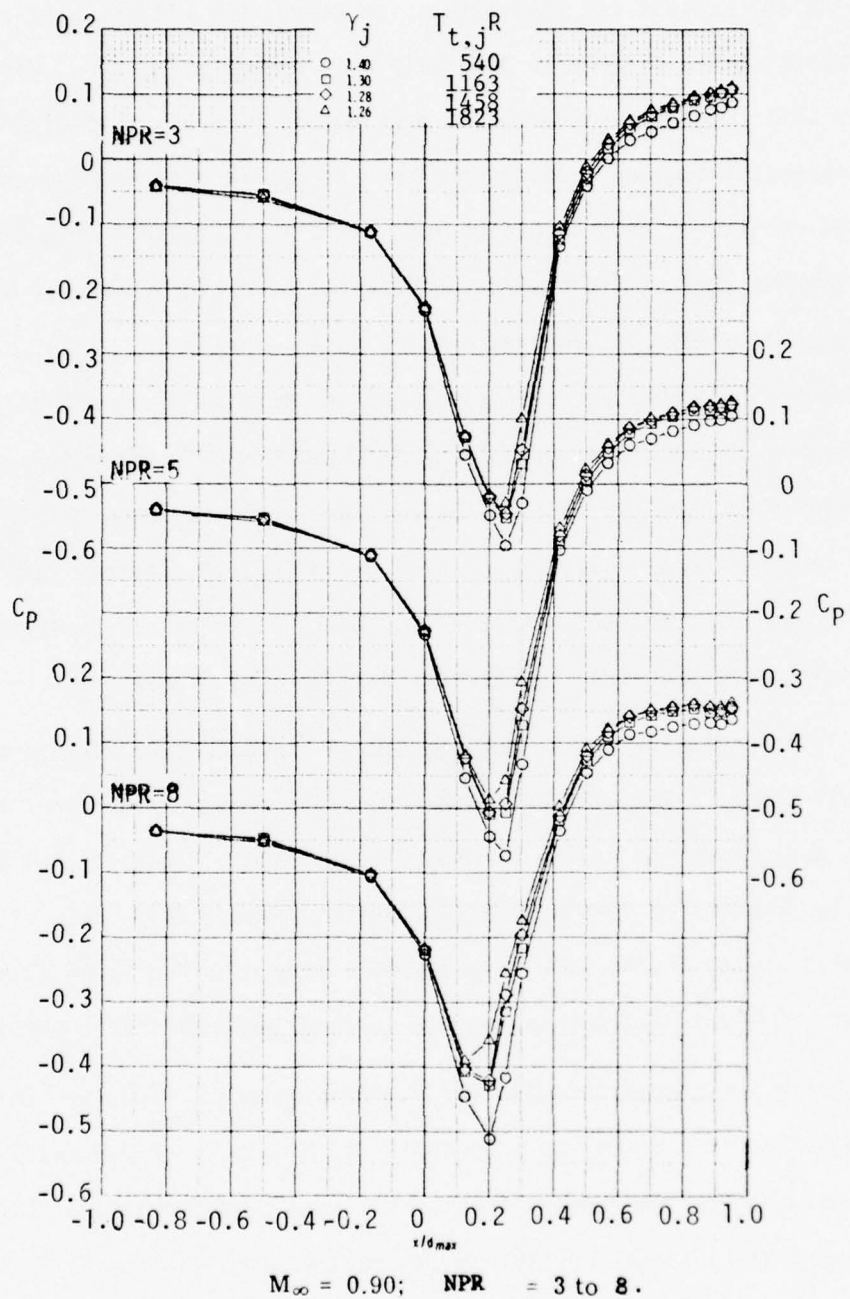


Figure 29. (Reference 2) Pressure Distribution for Hot Exhaust Jets

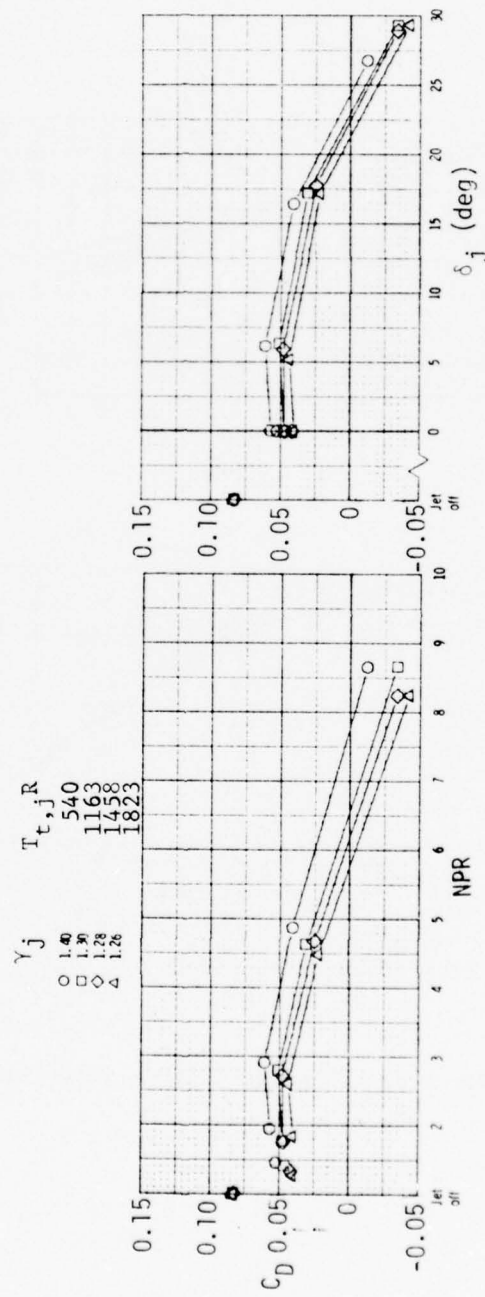
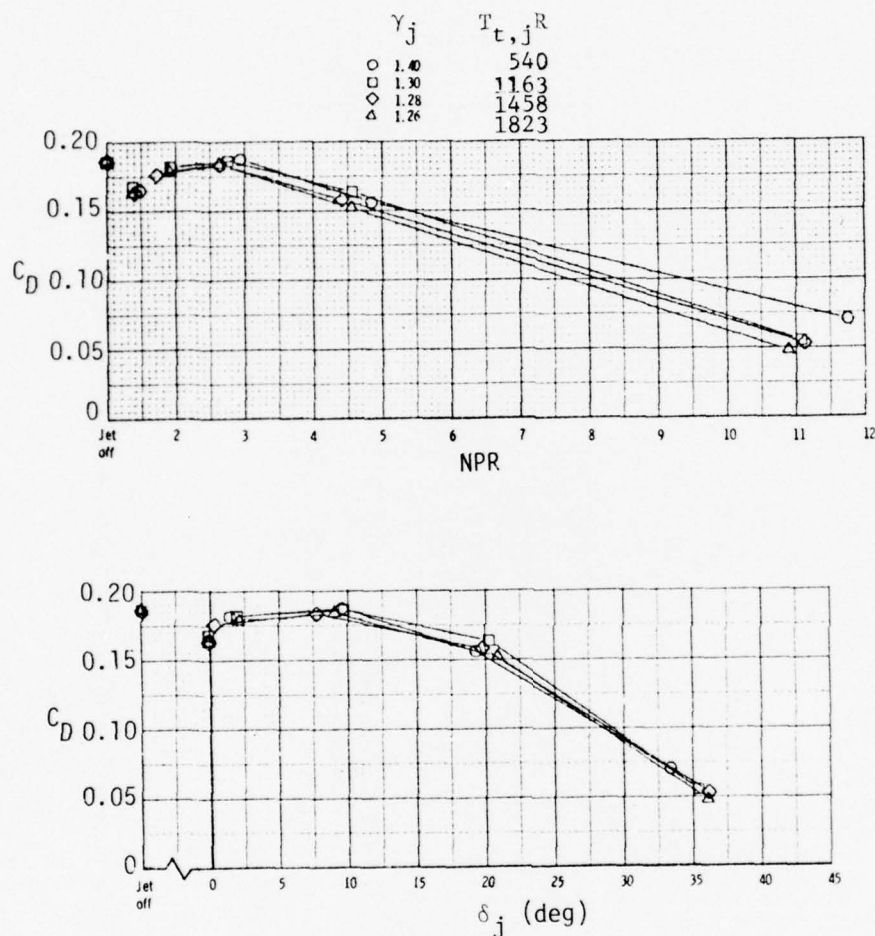


Figure 30. (Reference 2) Drag Coefficient Sensitivity,  $M_\infty = 0.90$

Figure 31. (Reference 2) Drag Coefficient Sensitivity,  $M_\infty = 1.20$

BEST AVAILABLE COPY

AFFDL-TR-76-138

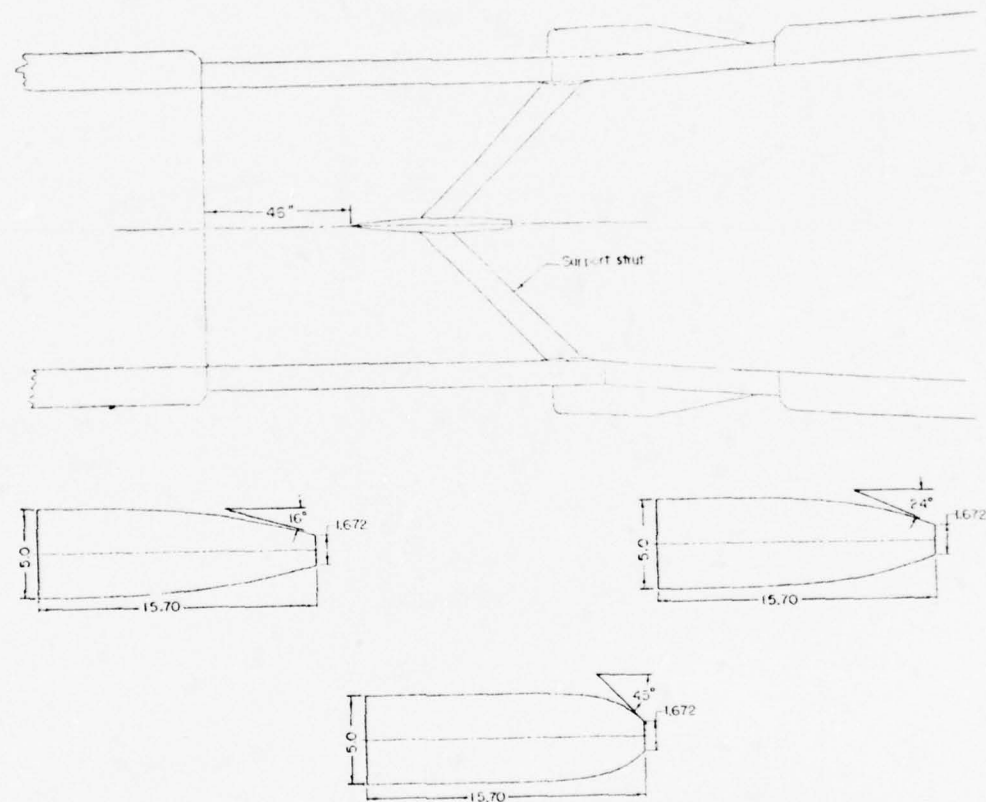


Figure 32. (Reference 8) Test Apparatus and Nozzle Models

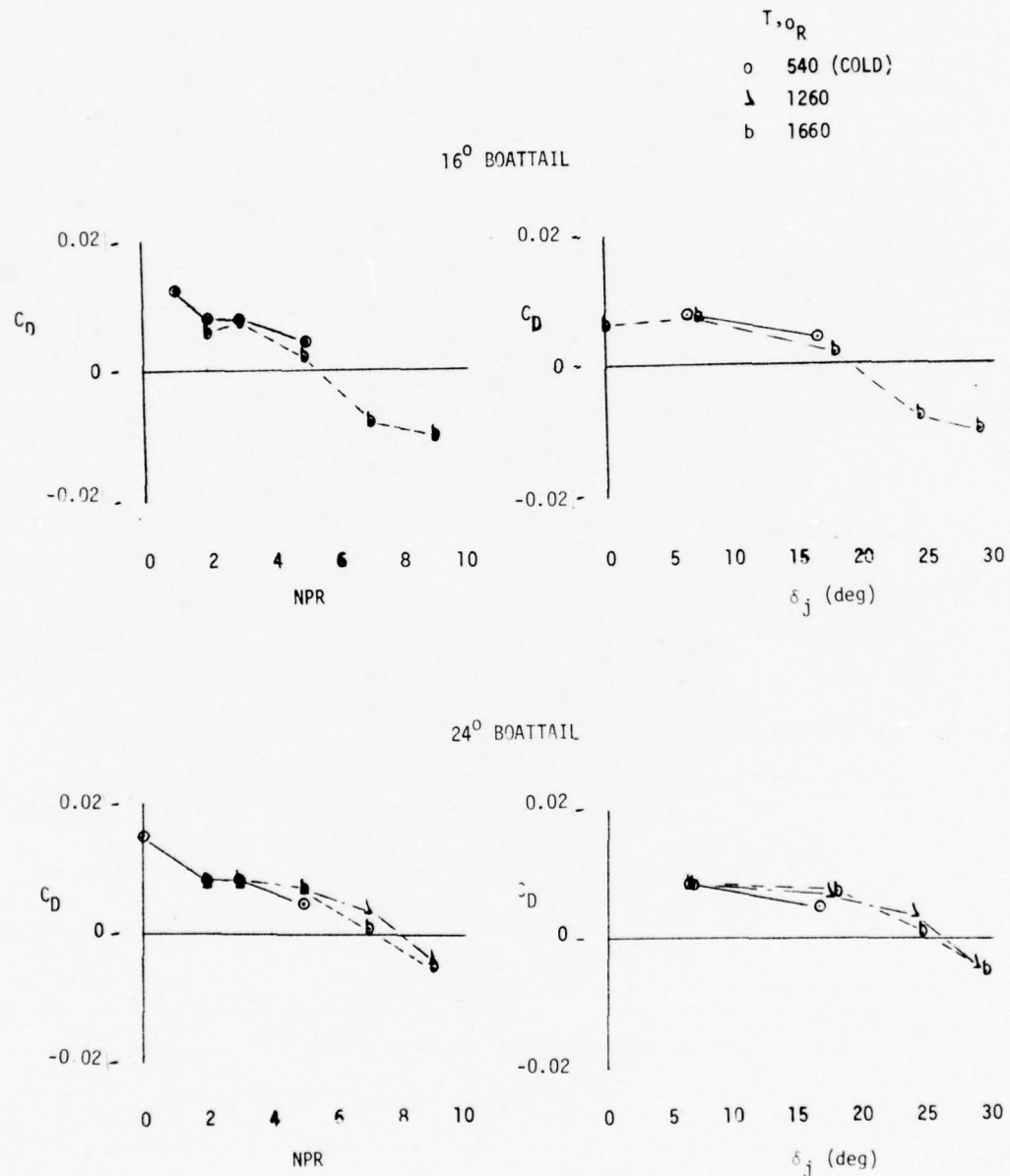


Figure 33. (Reference 8) Drag Coefficient vs. NPR and Initial Plume Angle Correlation,  $M_\infty = 0.8$

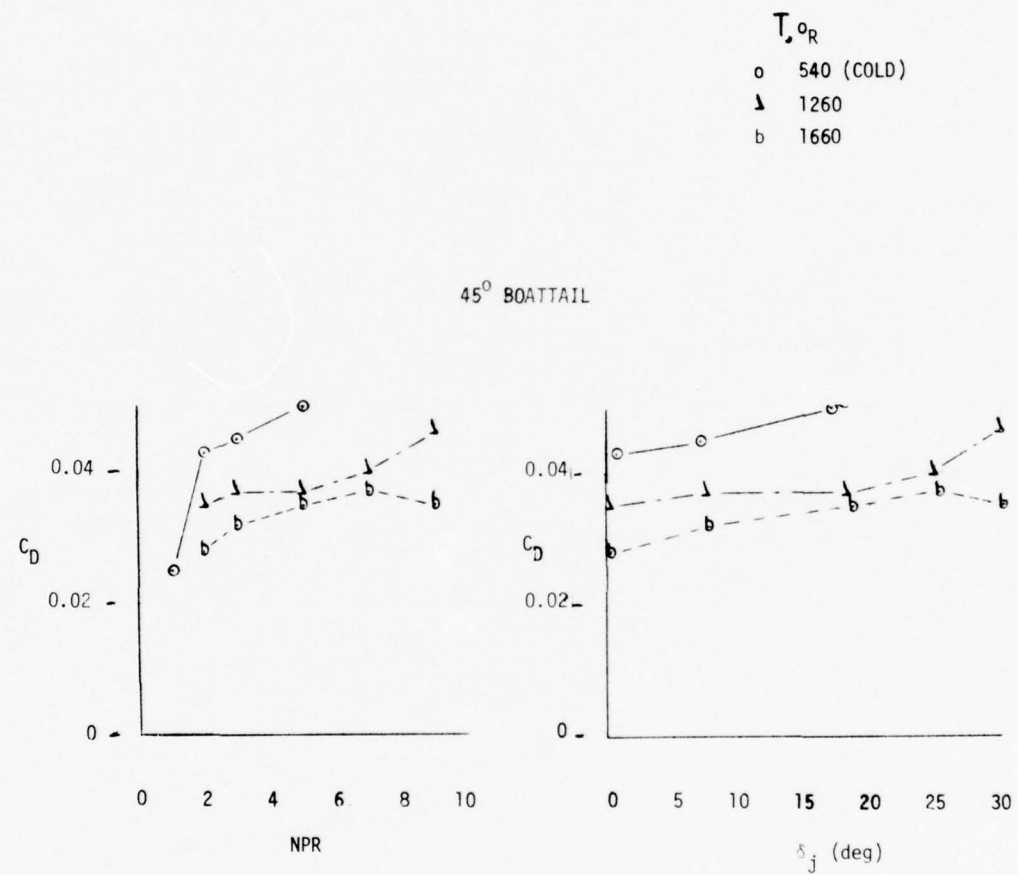


Figure 33 (Concluded)

$T, \text{o}_R$ 

o	540 (COLD)
▲	1260
b	1660

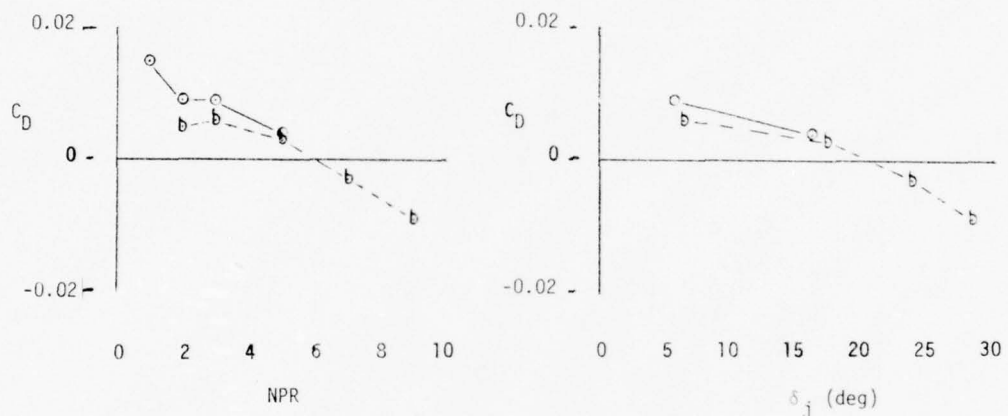
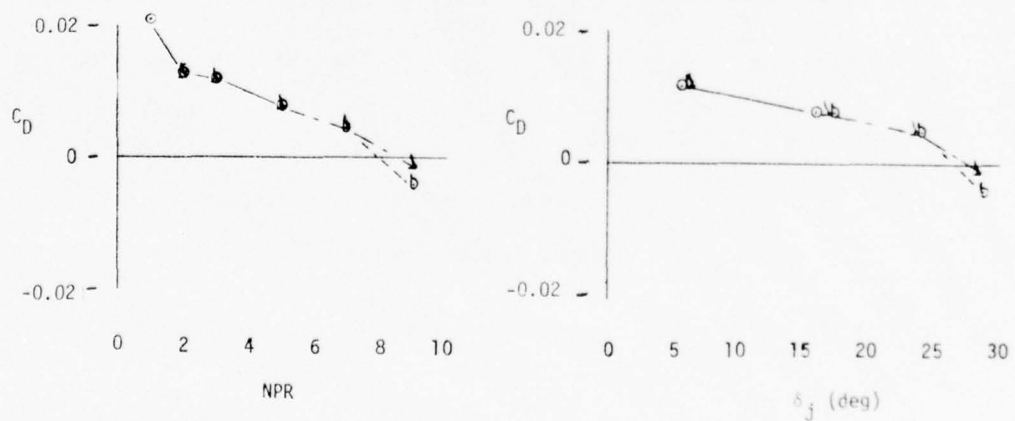
 $16^0$  BOATTAIL $24^0$  BOATTAIL

Figure 34. (Reference 8) Drag Coefficient vs. NPR and Initial Plume Angle Correlation,  $M_\infty = 0.9$

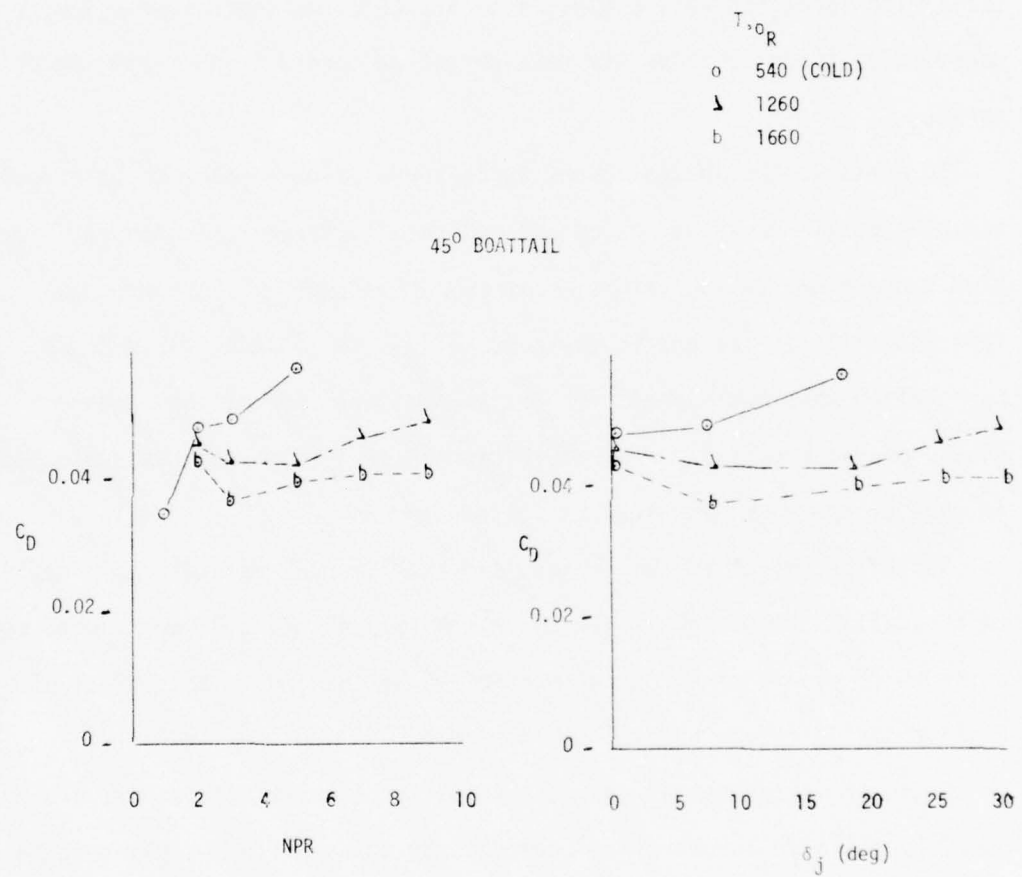


Figure 34 (Concluded)

the initial plume angle correlation tends to collapse the data together correcting for most if not all effects of the hot exhaust gas. For boattails with large boattail angles, i.e.  $\theta_{BT}=45^\circ$ , the initial plume angle correlation tends to leave the data spread unchanged or increase the data spread.

In summary, the initial plume angle correlation appears to be effective for high nozzle pressure ratios and moderate temperature increases. For high temperature exhaust flows, separated flow boattails, or attached flow boattails at low nozzle pressure ratios, the initial plume angle correlation does not correct for hot exhaust gas effects and in some cases, over-corrects the drag coefficient data. This trend is supported in part by the four data sources listed above.

While the amount of hot exhaust gas experimental data directly applicable to an initial plume angle analysis is limited, numerous other related sources exist which provide trends and information pertaining to the effect of a hot exhaust jet on nozzle boattail performance.

Ratio of specific heat changes as well as temperature changes are produced by a air/fuel combustion process. By using different gases in an exhaust jet, the  $\gamma$  variation can be produced without the accompanying temperature rise. Early efforts by NACA and NASA, References 10, 11, and 12, utilized cold air ( $\gamma=1.4$ ,  $T=540^\circ R$ ), heated air ( $\gamma=1.3$ ,  $T=2100^\circ R$ ), and a cold carbon dioxide jet ( $\gamma=1.3$ ,  $T=540^\circ R$ ). Lee, Reference 10, investigated jet plume shape and cold jet simulation of hot exhaust jets at transonic Mach numbers at the NASA Ames Research Center.

Primary instrumentation for the strut supported cone cylinder model with a convergent nozzle was Schlieren photographs and flow field pressure surveys.

Concerning the jet plume shape, the test results showed that for the hot air jet and the carbon dioxide jet, both with  $\gamma=1.29$ , the jet plume shape was similar at the nozzle exit and over most of one exhaust plume wavelength. The cold exhaust jet,  $\gamma=1.4$ , could be made to match the hot jet shape at the nozzle exit if the cold jet nozzle pressure ratio was increased. Downstream, however, the cold jet at an increased nozzle pressure ratio, did not match the hot jet plume shape. The result is that simulation of the hot jet boundary for at least one wavelength with a cold jet must be done at the same  $\gamma$  and nozzle pressure ratio. It was also found that the external shock wave location of the hot air jet could be matched by both the carbon dioxide jet and the cold exhaust jet.

The flow field static pressure surveys and the resulting forces and moments due to these pressure distributions indicated that the effect of temperature was small but the effect of the ratio of specific heats change was large. The hot air data and the carbon dioxide data are similar (same  $\gamma$ , different gas temperatures) while the cold air jet data is decidedly different (same gas temperature as carbon dioxide, different  $\gamma$ ).

The most pertinent result from this investigation is that the effect of a hot exhaust jet flow pattern is simulated by a cold jet if the nozzle pressure ratio and ratio of specific heats can be matched.

References 11 and 12 also investigated gases of different  $\gamma$ 's and the same temperature including heated air. Base and boattail pressures were measured on the model shown in Figure 35. The change in the base pressure coefficient for two gases at the same temperature but different  $\gamma$ 's is shown in Figure 36. Also shown is the effect on the base pressure coefficient of temperature and  $\gamma$  variations using air as a jet. In both cases, i.e. a smaller  $\gamma$  for the carbon dioxide gas than the cold air jet

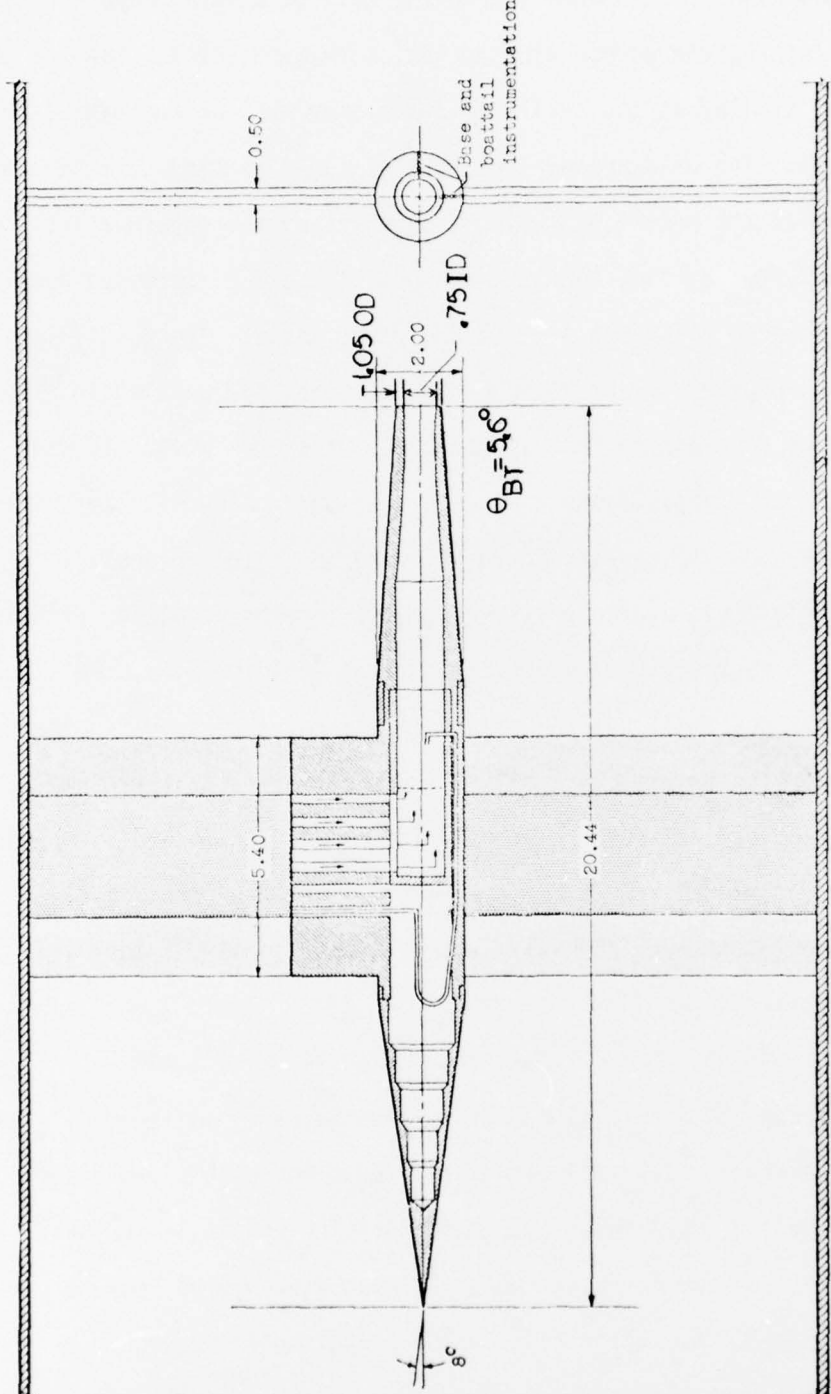


Figure 35. (Reference 12) Basic Model Details

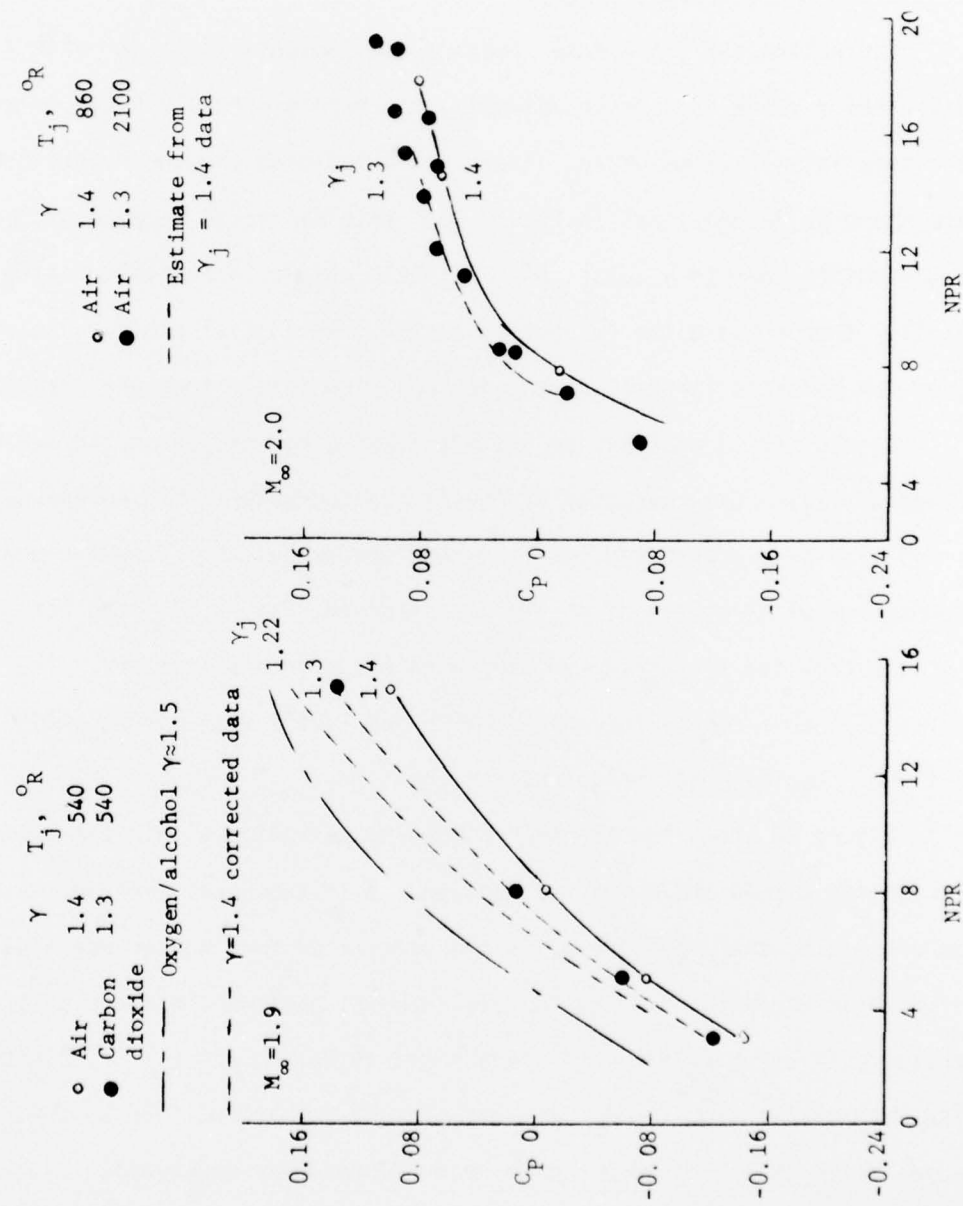


Figure 36. (Reference 11) Effect of  $\gamma$  and Temperature Variations on Base Pressure Coefficient

and the temperature and  $\gamma$  variations for a heated and cold air jet, the results were to increase the base pressure coefficient and therefore decrease the total aftbody drag.

Correcting the  $\gamma=1.4$  base pressure coefficients for a gas with a different  $\gamma$  value is done by adjusting the nozzle pressure ratio to give the same initial plume angle. These corrected base pressure coefficients are shown as dashed lines in Figure 36. This correction appears to be satisfactory down to  $\gamma$  values of 1.3. This result is consistent with earlier trends where the correction to the same initial plume angle was good for moderate temperature changes and high nozzle pressure ratios.

A quantitative analysis of the effect of a heated jet on the exhaust plume spreading was conducted by Rousso and Kochendorfer in Reference 13. Using a total pressure and total temperature probe, the exhaust plume downstream of a convergent nozzle was surveyed, Figure 37. The hot exhaust jet was provided by burning propane with the source plenum air. The primary chamber temperatures are  $540^0R$  and  $1400^0R$  with corresponding ratio of specific heat values of 1.4 and 1.35.

Figure 38 shows how the Mach number distribution within the plume varies for a cold and a hot exhaust jet.  $M$  is the local Mach number as determined by the probe and  $M_j$  is the calculated Mach number assuming an isentropic expansion from the nozzle internal pressure to the freestream pressure. A value of  $M/M_j=0.11$  is assumed to be the outer plume boundary. The Mach number profiles for the hot exhaust jet are similar to the cold jet in shape but show higher Mach numbers near the nozzle centerline. The effect of the hot jet on the Mach number profiles appears to diminish at downstream positions of the exhaust plume.

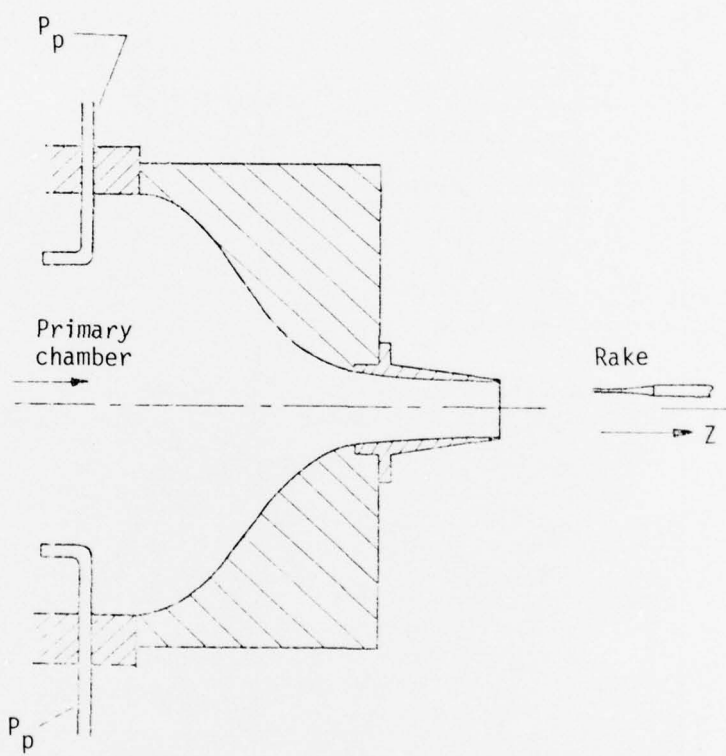


Figure 37. (Reference 13) Model Details and Rake Position

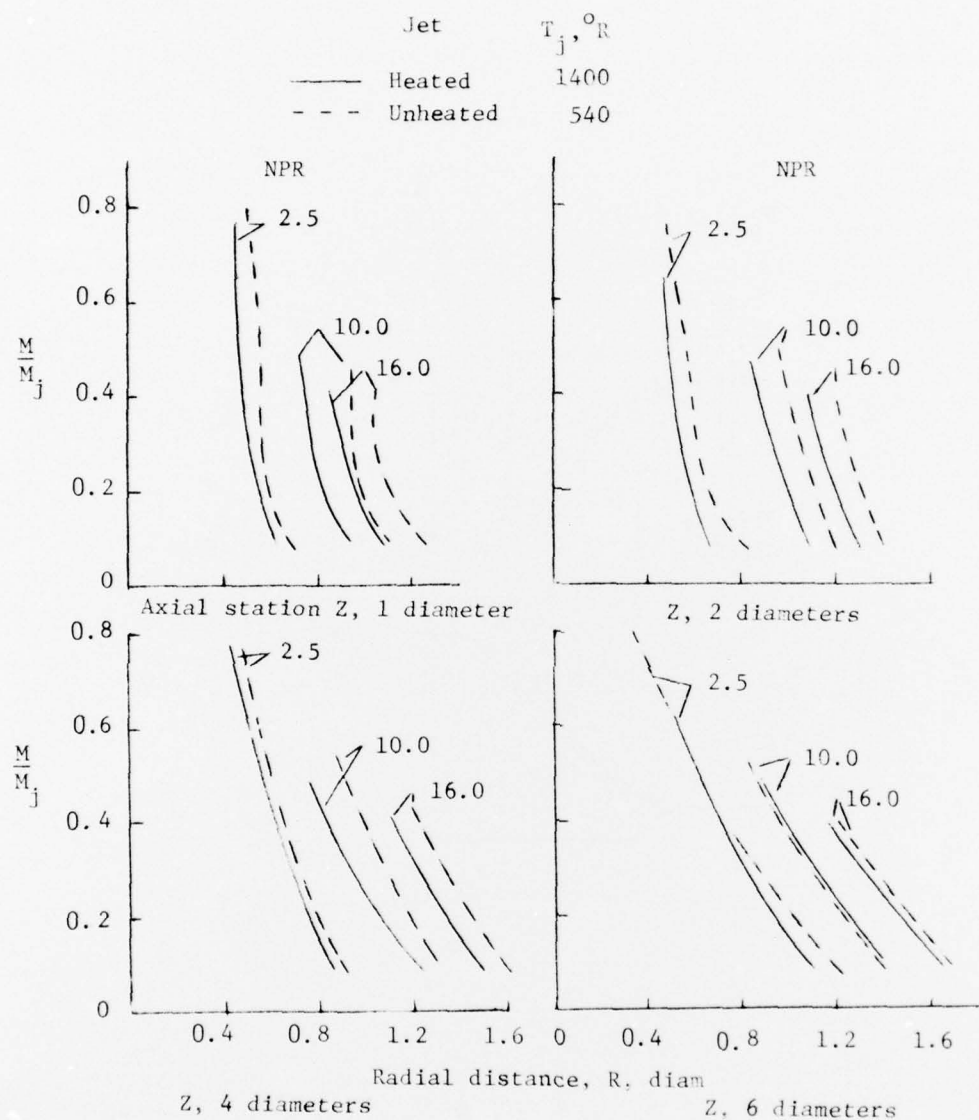


Figure 38 (Reference 13) Mach Number Profiles for Cold and Hot Exhaust Jets

An additional area for concern in hot exhaust testing of nozzle afterbody configurations is external nozzle surface heating. References 14 and 15, conducted for AGARD by German and Netherland research agencies respectively, show that uncooled nozzle aftbody models can produce anomalies when investigating the effect of a hot exhaust jet on the nozzle drag coefficient.

In Reference 14, the model is a HFB 320, a commercial transport nacelle. Primary instrumentation is external static pressure orifices and surface thermocouples. Exhaust gas temperatures range from  $522^0R$  to  $1422^0R$ . The variation of nozzle drag coefficient with Mach number and temperature is shown in Figure 39. The higher nozzle drag coefficient for the hot jet case than the cold jet is opposite of trends experienced in other test facilities. The anomaly appears to be a result of body heating by the exhaust jet. The body surface temperature, recorded by the surface thermocouples, is approximately the jet exhaust temperature of  $1422^0R$ . This model boundary layer temperature gradient creates an outward flow from the model. This modifies the boundary layer profiles to a more turbulent shape and effectively creates a "blown" boundary layer. The more turbulent boundary layer for the heated body results in less re-compression (Figure 40) on the aftbody and therefore more drag for a hot jet than a cold jet.

Reference 15 also shows the effect of body heating tends to reverse the previous trends of nozzle aftbody drag coefficient with exhaust gas temperature. For this data, however, the anomaly does not exist above nozzle pressure ratios of 3, Figure 41.

Both of these references indicate that as a testing technique, care must be taken to avoid compromising the external nozzle pressure data by nozzle surface heating.

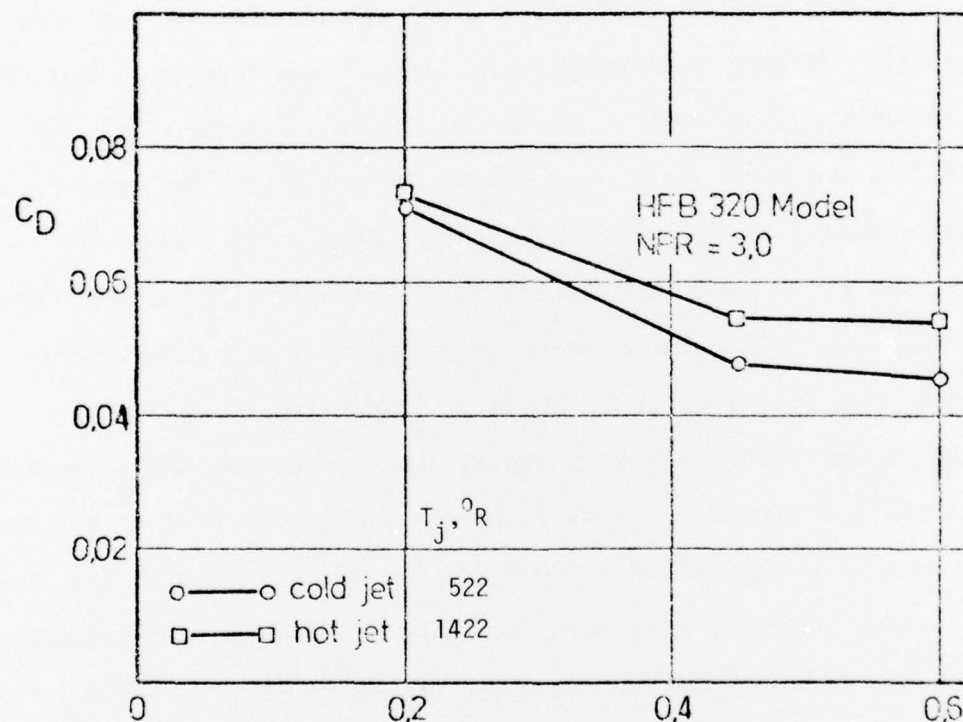


Figure 39. (Reference 14) Drag Coefficient Sensitivity with Temperature

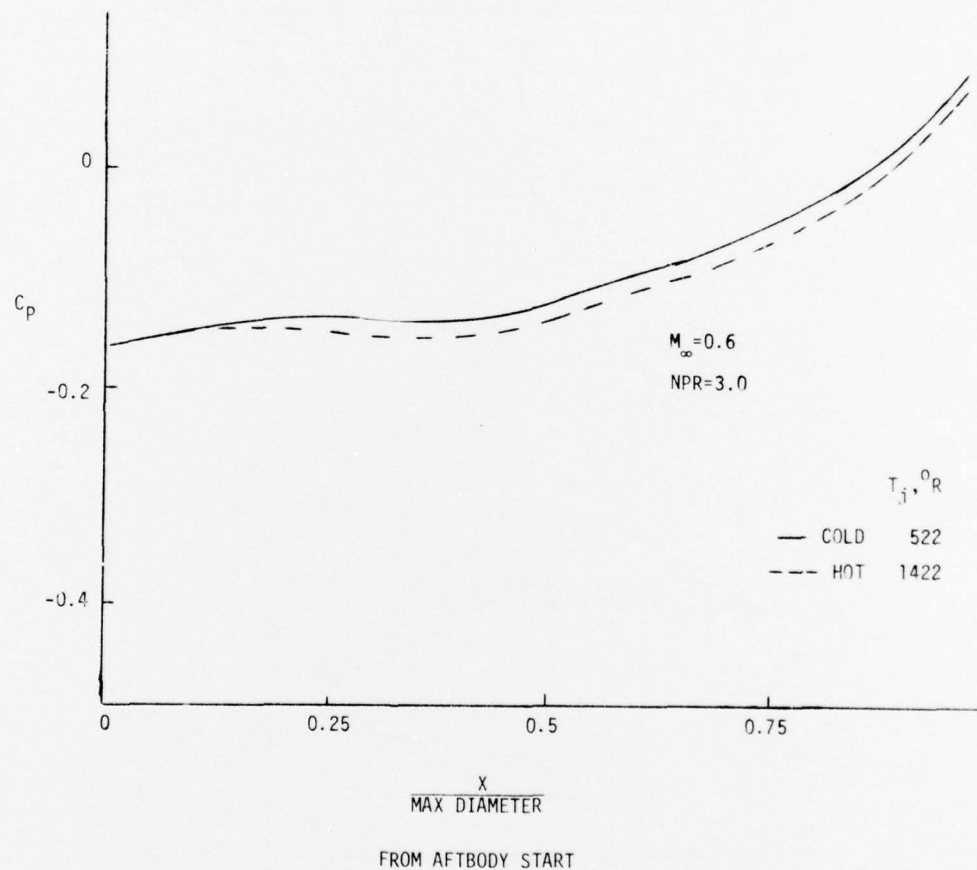


Figure 40. (Reference 14) External Nozzle Aftbody Pressure Coefficient Distribution Variations with Exhaust Plume Temperature

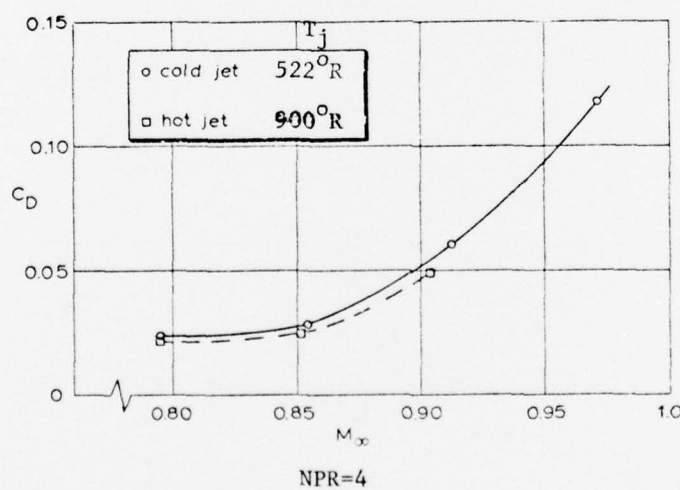
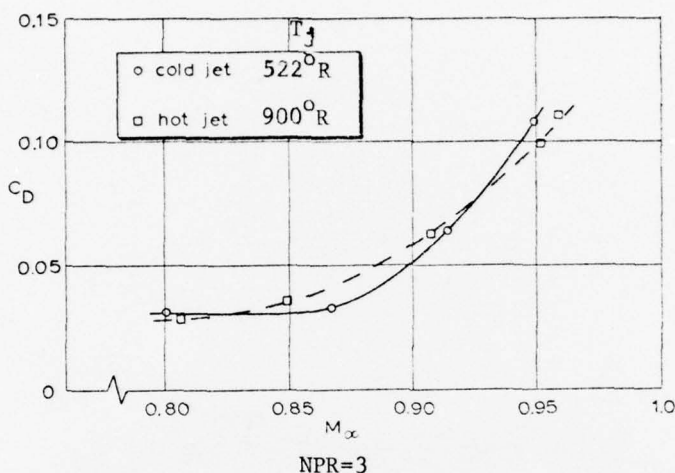


Figure 41. (Reference 15) Drag Coefficient Sensitivity with Exhaust Jet Temperature

### SECTION III

#### SUMMARY

The application of the initial plume angle as a correlating factor for hot exhaust gas effects for nozzle/aftbody pressure drag has been investigated over an extensive data base. In addition, general testing techniques and flow characteristics for hot exhaust gas simulation have been summarized. The summary of results of this effort are as follows:

1. As the exhaust gas temperature increases, the aftbody nozzle pressure drag decreases for cooled models. For uncooled models where the model surface temperature increases with increasing exhaust gas temperature, the trend with exhaust gas temperature is to increase the nozzle aftbody drag. This is a result of temperature changes in the boundary layer and its effect on the flow pattern.

2. The initial plume angle correlation successfully accounts for hot exhaust gas effects on nozzle aftbody drag if:

- a. the aftbody boattail angle is low to moderate, i.e. up to  $15^{\circ}$  and
- b. the nozzle pressure ratio is moderate to high, i.e.  $NPR > 6$ , and
- c. the temperature range is not large between the cold flow exhaust gas and the hottest exhaust gas, i.e.  $540^{\circ}R$  and  $2000^{\circ}R$ .

3. The initial plume angle correlation fails to account for hot exhaust gas effects on nozzle aftbody drag if:

- a. the aftbody has a large boattail angle,  $\theta_{BT} = 25^{\circ}$  or greater, where the external flow is separated and nozzle pressure drag is not sensitive to changes in nozzle pressure ratio, or

- b. the nozzle pressure ratio is below moderate values, i.e.  $NPR < 6$ , (operating nozzle pressure ratios for existing turbojet/turbofan engines is approximately 2.5 to 6) or
- c. the temperature difference is large between the cold jet and the highest exhaust gas temperature, e.g. if  $\Delta T > 2000^{\circ}R$ .

4. For aftbodies where the exhaust gas temperature effect on aftbody drag is small, the initial plume angle correlation may over-correct for the hot gas drag coefficient data.

5. Simulation of the hot plume boundary for at least one plume wave length may be made by a cold gas at the same  $\gamma$  and nozzle pressure ratio as the hot exhaust gas.

6. The initial plume angle correlation treats the plume as a solid body. The correlation fails in areas where jet entrainment and mixing are important parameters. The initial plume angle correlation when combined with a correlating factor for jet entrainment and mixing may offer a better technique for correcting cold jet aftbody pressure drag for hot exhaust gas effects.

BIBLIOGRAPHY

Sources Related to the Effects of Exhaust  
Gas Temperature or Ratio of Specific Heats  
Variations on Aftbody/Nozzle Flow

Beke, A., Simon, P. C., Thrust and Drag Characteristics of Simulated Variable Shroud Nozzles With Hot and Cold Primary Flows at Subsonic and Supersonic Speeds, NACA RM E54J26, February 1955.

Bressette, W. E., Some Experiments Relating To The Problem Of Simulation Of Hot Jet Engines In Studies Of Jet Effects On Adjacent Surfaces At A Free-Stream Mach Number Of 1.80, NACA RM L56E07, July 1956.

Englert, G. W., Operational Method of Determining Initial Contour of and Pressure Field About a Supersonic Jet, NASA TN D-279, April 1960.

Hearth, D. P., Wilcox, F. A., Thrust and Drag Characteristics of A Convergent-Divergent Nozzle with Various Exhaust Jet Temperatures, NACA RM E53L23b, March 1954.

Love, E. S., Initial Inclination of the Mixing Boundary Separating An Exhausting Supersonic Jet From A Supersonic Ambient Stream, NACA RM L55J14, 1955.

NACA Conference On Aircraft Propulsion Systems, Volume I, NASA-TMX-67171, December 1955.

NACA 1957 Flight Propulsion Conference, NASA-TMX-67368, November 1957.

Norton, H. T., Swihart, J. M., Effect of A Hot-Jet Exhaust on Pressure Distributions and External Drag of Several Afterbodies On A Single-Engine Airplane Model At Transonic Speeds, NACA RM L57J04, March 1958.

Reubush, D. C., Experimental Study of the Effectiveness of Cylindrical Plume Simulators For Predicting Jet-On Boattail Drag at Mach Numbers Up To 1.30, NASA TND-7795, November 1974.

Walker, S. C., Nozzle-Afterbody Wind Tunnel Test of an Attack Aircraft, AD-921 462L, LTV Aerospace Corporation, April 1974.

REFERENCES

1. Robinson, C. E., High, M. D., Exhaust Plume Temperature Effects on Nozzle Afterbody Performance Over the Transonic Mach Number Range, AEDC-TR-74-9, U. S. Air Force, July 1974.
2. Compton, William B., Effects of Jet Exhaust Gas Properties on Exhaust Simulation and Afterbody Drag, NASA-TR-R-444, National Aeronautics and Space Administration, October 1975.
3. Love, Eugene S., Grigsby, Carl E., Some Studies of Axisymmetric Free Jets Exhausting From Sonic and Supersonic Nozzles Into Still Air and Into Supersonic Streams, NACA RM L54L31, 1954.
4. Love, Eugene S., Woodling, Mildred J., Lee, Louise P., Boundaries of Supersonic Axisymmetric Free Jets, NACA RM L56G18, 1956.
5. Love, Eugene S., et. al., Experimental and Theoretical Studies of Axisymmetric Free Jets, NASA TR R-6, 1959.
6. Bergman, David, Effects of Engine Exhaust Flow on Boattail Drag, AIAA Paper 70-132, January 1970.
7. Glasgow, Edsel R., et. al., Integrated Airframe-Nozzle Performance For Designing Twin-Engine Fighters, AFFDL-TR-73-71, June 1973.
8. Henry, B. Z., Cahn, M. S., Preliminary Results of an Investigation at Transonic Speeds to Determine the Effects of a Heated Propulsive Jet on the Drag Characteristics of a Related Series of Afterbodies, NACA RM L55A24a, March 1955.
9. Galigher, L. L., Jackson, F. M., Robinson, C. E., Description of the AGARD Nozzle Afterbody Experiments Conducted by the Arnold Engineering Development Center, AGARDograph No. 208, Improved Nozzle Testing Techniques In Transonic Flow, September 1974.
10. Lee, G., An Investigation of Transonic Flow Fields Surrounding Hot and Cold Sonic Jets, NASA TND-853, April 1961.
11. Cortright, E. M., Kochendorfer, F. D., Jet Effects on Flow Over Afterbodies in Supersonic Stream, NACA RM E53H25, 1953.
12. Baughman, L. E., Kochendorfer, F. D., Jet Effects on Base Pressures of Conical Afterbodies At Mach 1.91 and 3.12, NACA RM E57E06, August 1957.
13. Rousso, M. D., Kochendorfer, F. D., Velocity and Temperature Fields in Circular Jet Expanding from Choked Nozzle Into Quiescent Air, NACA RM E51F18, July 1951.

REFERENCES (CONCLUDED)

14. Dissen, H., Zacharias, A., An Experimental Study of the Influence of the Jet Parameters on the Aftbody Drag of a Jet Engine Nacelle Scale Model, AGARDograph No. 208, Improved Nozzle Testing Techniques In Transonic Flow, September 1974.
15. Rozendaal, D., Groothoff, C. C., Derksen, W. B., Results of NLR Contribution to AGARD AD HOC Study, AGARDograph No. 208, Improved Nozzle Testing Techniques In Transonic Flow, September 1974.